

Parallel Algorithms for Combined Regularized Support Vector Machines: Application in Music Genre Classification

Rongmei Liang*,
Zizheng Liu[†], Xiaofei Wu[‡],
Jingwen Tu[§]

Abstract

In the era of rapid development of artificial intelligence, its applications span across diverse fields, relying heavily on effective data processing and model optimization. Combined Regularized Support Vector Machines (CR-SVMs) can effectively handle the structural information among data features, but there is a lack of efficient algorithms in distributed-stored big data. To address this issue, we propose a unified optimization framework based on consensus structure. This framework is not only applicable to various loss functions and combined regularization terms but can also be effectively extended to non-convex regularization terms, showing strong scalability. Based on this framework, we develop a distributed parallel alternating direction method of multipliers (ADMM) algorithm to efficiently compute CR-SVMs when data is stored in a distributed manner. To ensure the convergence of the algorithm, we also introduce the Gaussian back-substitution method. Meanwhile, for the integrity of the paper, we introduce a new model, the sparse group lasso support vector machine (SGL-SVM), and apply it to music information retrieval. Theoretical analysis confirms that the computational complexity of the proposed algorithm is not affected by different regularization terms and loss functions, highlighting the universality of the parallel algorithm. Experiments on synthetic and free music archiving datasets demonstrate the reliability, stability, and efficiency of the algorithm.

Keywords: Big data analytics, Combined regularization term, Support vector machine, Music genre classification.

1 Introduction

Against the backdrop of the big-data-driven era, machine learning encounters significant challenges in terms of computation and storage (Boyd et al. (2010) and Li et al. (2025)). The data, with its extremely large volume, often cannot be entirely stored on a single machine (Wu et al. (2025b) and Wu et al. (2025c)). Furthermore, in numerous applications, individual agents such as local governments, research laboratories, hospitals, and smartphones independently collect data. Due to the limited bandwidth, communication costs are prohibitively high. Moreover, direct data sharing raises concerns regarding

*Department of Statistics and Data Science, Southern University of Science and Technology, Guangdong, 518055, P.R. China. Email: liang_r_m@163.com

[†]Liu and Liang contributed equally to this paper. Faculty of Education, Languages, Psychology & Music, SEGi University, Kuala Lumpur, 47810, Malaysia. Email: liuzizheng199608@163.com

[‡]College of Mathematics and Statistics, Chongqing University, Chongqing 401331, P.R. China. E-mail: xfwu1016@163.com

[§]Corresponding author. School of Mathematical and Physical Sciences, Chongqing University of Science and Technology, Chongqing 401331, P.R. China. Email: 15310293521@163.com

privacy and the loss of data ownership. In this context, distributed parallel computing has become the core paradigm for processing massive high-dimensional data and breaking through the performance bottlenecks of single machines.

This imperative is particularly evident in fields like Music Information Retrieval (MIR), where the explosion of digital music data presents a quintessential example of “big data” challenges. Modern MIR tasks involve analyzing audio signals that are intrinsically high-dimensional, temporally sequential, and semantically structured. The acoustic features extracted from music—such as spectral, rhythmic, and harmonic descriptors—often exhibit rich underlying structures; they form natural groups, such as MFCCs collectively representing timbre and display strong temporal dependencies across consecutive audio frames. This complex data structure renders conventional sparse models inadequate, as they fail to leverage the grouped and sequential relationships among features, which are crucial for accurate music characterization.

Therefore, this paper focuses on a highly challenging yet practically significant problem: designing distributed parallel algorithms for combined regularized Support Vector Machines (CR-SVMs). The non-smooth hinge loss, coupled with complex composite regularization terms designed to encode structural priors, such as sparsity, group sparsity and temporal smoothness, presents a formidable optimization problem. This challenge is drastically amplified under data-distributed scenarios, where classical optimization techniques falter. By addressing this gap, our work aims to provide a scalable and efficient computational framework that unlocks the full potential of structured SVMs for large-scale, structurally rich datasets like those in MIR.

As a powerful classification tool, SVM proposed by Vapnik (1995) has been widely applied in various fields such as maintenance of industrial machines (Langone et al. (2015)), music emotion recognition (Xing et al. (2015)) and image recognition (Du et al. (2016b)). Its basic principle is to find an optimal hyperplane in the feature space that can maximize the margin between different classes of data points. In the case of linearly separable data, SVM tries to find a hyperplane that can perfectly separate the two classes with the largest possible distance from the nearest data points of each class. For non-linearly separable data, SVM maps the original data into a higher dimensional space through a kernel function, where the data becomes linearly separable.

Given a data set $\{\mathbf{X}, \mathbf{y}\} = \{(\mathbf{x}_i, y_i)\}_{i=1}^n$, where $\mathbf{x}_i \in \mathbb{R}^p$ and $y_i \in \{-1, +1\}$, the traditional SVM can be expressed as:

$$\min_{\boldsymbol{\beta}, \beta_0} \frac{1}{n} \sum_{i=1}^n [1 - y_i (\sum_{j=1}^p x_{ij} \beta_j + \beta_0)]_+ + \frac{\lambda}{2} \|\boldsymbol{\beta}\|_2^2, \quad (1.1)$$

where λ is tuning parameter, the $(\boldsymbol{\beta}, \beta_0)$ pair is the decision variable with $\boldsymbol{\beta} \in \mathbb{R}^p$ and $\beta_0 \in \mathbb{R}$, $[1 - y_i (\sum_{j=1}^p x_{ij} \beta_j + \beta_0)]_+$ is the hinge loss function for SVM with $[r]_+ = \max\{r, 0\}$.

Most of the existing research on SVM models mainly focuses on the sparsity of data. For example, ℓ_1 -norm SVM (Zhu et al. (2003)), the smoothly clipped absolute deviation (SCAD) penalized SVM (Becker et al. (2011)) and minimax concave penalty (MCP) penalized SVM (Zhang et al. (2016)) are proposed to promote sparsity in the model. Sparsity is beneficial as it can reduce the complexity of the model and improve its interpretability. However, this research, which promotes mere sparsity, is insufficient to capture the intricate structures inherent in data like music signals. For example, in music signal analysis, audio features often form natural groups based on their acoustic properties, such as spectral features, rhythmic features, and harmonic features. Moreover, the relationships within and between these groups

contain valuable information for music characterization. In musical time-series data, such as a sequence of audio frames, consecutive features exhibit strong temporal dependencies. The research significance of combined regularization terms—which can simultaneously induce sparsity while respecting feature groups and temporal coherence—therefore far exceeds that of simple sparsity research, motivating the core algorithmic contributions of this work.

Commonly used combined regularization terms (CRTs) include Elastic net (EN, [Zou and Hastie \(2005\)](#)), Sparse fused Lasso (SFL, [Tibshirani et al. \(2005\)](#)), and Sparse group Lasso (SGL, [Friedman et al. \(2010\)](#)). Applying combined regularization terms to SVM models, can not only improve the generalization ability of models but also enhance their flexibility and adaptability, which is of high research value. Let us review the relevant work on CR-SVMs.

- **SVM with elastic net (EN-SVM):** The EN regularization, a linear combination of the ℓ_1 and ℓ_2 norm, encourage highly correlated features to be selected or removed together. It is defined as

$$\lambda_1 \|\boldsymbol{\beta}\|_1 + \lambda_2 \|\boldsymbol{\beta}\|_2^2. \quad (1.2)$$

[Wang et al. \(2006\)](#) replaced ℓ_1 norm in (1.1) with EN regularization to obtain the EN-SVM. Meanwhile, a corresponding algorithm based on least angle regression (LAR) was also presented to compute the complete solution path of DrSVM. [Yang and Zou \(2013\)](#) introduced a generalized coordinate descent (GCD) algorithm for solving a class of elastic net penalized SVMs. [Xu et al. \(2015\)](#) investigated the application of the proximal gradient (PG) method in solving the elastic net penalized huberized SVM. In addition, [Zhu et al. \(2020\)](#) employed the proximal gradient algorithm to solve the huberized pinball elastic-net SVM (HPSVM). [Liang et al. \(2024\)](#) introduced a linearized ADMM to solve EN-SVM.

- **SVM with sparse fused lasso (SFL-SVM):** The SFL regularization, a linear combination of the ℓ_1 norm and total variation, encourages sparsity of the coefficients and also sparsity of their differences. It is defined as

$$\lambda_1 \|\boldsymbol{\beta}\|_1 + \lambda_2 \sum_{j=2}^p |\beta_j - \beta_{j-1}|. \quad (1.3)$$

The SFL-SVM was initially introduced by [Tibshirani et al. \(2005\)](#), who incorporated quadratic programming techniques for its solution. [Ye and Xie \(2011\)](#) devised an iterative algorithm grounded in the split Bregman method to tackle a class of large-scale fused Lasso problems, which encompasses a generalized fused Lasso and SFL-SVM. [Wu et al. \(2024\)](#) formulated a multi-block ADMM algorithm for quantile fused Lasso. This algorithm can be readily extended to SFL-SVM. [Wu et al. \(2025d\)](#) presented a pinball SVM with SFL and developed a unified multi-block linearized ADMM algorithm for its resolution.

- **SVM with sparse group lasso (SGL-SVM):** To the best of our knowledge, the current research on SGL-SVM is limited to the two-step classification method proposed by [Huo et al. \(2020\)](#). In this method, sparse group Lasso serves the purpose of variable selection initially, followed by the utilization of SVM for classification. As of now, there is no systematic and formal research results have been reported. In this paper, we will present the specific expression of SGL-SVM in Section 2.1.

Although the algorithms of EN-SVMs and SFL-SVMs have been extensively studied, most of the existing works have certain limitations. For instance, the LAR and quadratic programming algorithms are ineffective in dealing with high-dimensional problems. The GCD and the PG algorithm cannot handle non-differentiable loss functions. In summary, there is currently no algorithm that can effectively solve

the high-dimensional CR-SVMs problem when the data is stored in a distributed fashion. The main work of this paper is to fill this gap and develop an efficient parallel algorithm for high-dimensional CR-SVMs. Our contributions can be summarized as follows:

1. We introduce an SVM model integrated with the SGL, named SGL-SVM. When confronted with grouped data, it is capable of attaining sparsity concurrently at both the group and individual feature scales. This dual-level sparsity property empowers the SGL-SVM to effectively identify and select not only the most relevant groups but also the most significant predictors within each chosen group. We also applied the model to music gene classification. Experiments have demonstrated that the model can automatically perform feature group selection, identify the acoustic feature categories that are most discriminative for the classification task, thereby enhancing the interpretability of model and aligning it with musicological cognition.
2. We develop a unified consensus-based parallel ADMM algorithm for high-dimensional CR-SVMs. Due to the presence of the intercept term β_0 in the SVM, the proposed algorithm cannot be transformed into a two-block ADMM algorithm, but only a three-block one. To ensure the convergence of the algorithm, we carefully arranged the order of variable iteration and applied the Gaussian back substitution technique to refine the iterative results. As a result, the proposed parallel ADMM algorithm achieves an improved sublinear convergence rate.
3. We validated our proposed algorithm on the publicly available benchmark dataset FMA (Free Music Archiv) in the field of music information retrieval. The numerical experimental results show that SGL-SVM perform better than those without grouping. When collecting the audio data of these songs, grouping the features according to the inherent characteristics of the audio data features can help the trained machine learning model predict the categories of newly collected songs. The data experiments also indicate that when training the SGL-SVM, among the seven types of audio features, the group of MFCC features plays the most important role, followed by the group of spectral features, and then the group of chroma features. The remaining four groups of features have little effect. This implies that when classifying a large volume of music data with limited machine memory, simply collecting the three variable sets selected by the proposed SGL-SVM can not only save data storage space but also enable the automatic implementation of music data classification using machine learning models.

The rest of this paper is organized as follows. In Section 2, we introduce SGL-SVM and extend the sparse group Lasso regularization to a variety of more general combined regularization terms. Based on this, we propose a unified expression framework for diverse CR-SVM models. Building upon this framework, Section 3 designs a distributed algorithm and offer the convergence analysis. The validation of the performance of the algorithm is the core of Section 4. Here, we utilize both simulated and real-world data to verify the feasibility, efficiency, and accuracy of the algorithm. In Section 5, we wrap up the paper by summarizing the major findings and conclusions. Additionally, we engage in a discussion about the potential directions for future research. Technical proof are provided in the supporting material. We put the R codes for implementing the proposed parallel algorithm and reproducing our experiments on <https://github.com/xfwu1016/PADMM-for-Svms>.

2 Preliminaries

Here, we introduce SGL-SVM and extend the sparse group Lasso regularization to a variety of more general combined regularization terms.

2.1 SGL-SVM

In numerous modern applications, data collected from multiple sources often exhibit a natural grouped structure, where features generated from the same source form a coherent unit. This characteristic is exceptionally prominent in the field of MIR. For instance, in music production, a multi-track recording consists of individual tracks for different instruments such as drums, guitar and vocals. Features extracted from the same instrument track inherently constitute a distinct group. Similarly, low-level and high-level features extracted from an audio signal can be categorically organized into groups such as spectral features, rhythmic features, and harmonic features. These groups capture different facets of musical information, and the relationships within and between them are crucial for comprehensive music characterization.

Confronted with such pervasively grouped data, traditional SVMs struggle to fully leverage this inherent group-structure information. This often leads to an inability to effectively identify important feature groups, thereby impairing the model’s performance and interpretability. Although prior research has attempted to incorporate group feature selection into SVMs—for example, the Bayesian group feature selection framework based on pseudo-likelihood and data augmentation proposed by [Du et al. \(2016a\)](#), and the group feature selection in multiclass SVM considered by [Tang et al. \(2018\)](#), significant limitations remain when these methods are directly applied to complex, structured data like music features. A primary shortcoming is that these approaches typically achieve sparsity only at the group level; that is, if a feature group is selected, all coefficients within that group become non-zero. However, in musical analysis, we often desire sparsity concurrently at both the group and the individual feature levels. For example, we may wish to identify that “spectral features” as a whole group is relevant for genre classification, but within that group, only a few key predictors, such as “spectral contrast” and “spectral flux”, are truly significant, while others are redundant.

To achieve this dual-level sparsity, we focus on the SGL-SVM. Support the p -vector β is partitioned into M disjoint groups denoted respectively by $\beta_{(1)}, \beta_{(2)}, \dots, \beta_{(M)}$, then the SGL regularization is defined as

$$\lambda_1 \|\beta\|_1 + \lambda_2 \sum_{m=1}^M \|\beta_{(m)}\|_2 = \lambda_1 \|\beta\|_1 + \lambda_2 \|\beta\|_{2,1} \quad (2.1)$$

where $\ell_{2,1}$ -norm is a rotational invariant of the ℓ_1 norm. We can obtain SGL-SVM by replacing ℓ_1 norm in (1.1) with SGL regularization, which can be presented as

$$\min_{\beta, \beta_0} \frac{1}{n} \sum_{i=1}^n [1 - y_i (\sum_{j=1}^p x_{ij} \beta_j + \beta_0)]_+ + \lambda_1 \|\beta\|_1 + \lambda_2 \|\beta\|_{2,1}. \quad (2.2)$$

This model is uniquely empowered to simultaneously select impactful groups and the most significant features within those groups, making it exceptionally suitable for analyzing high-dimensional data with inherent group structures, such as music features. Despite this compelling suitability, research dedicated to applying and optimizing SGL-SVM specifically for MIR tasks is remarkably scarce. The work presented in this paper aims to fill this gap by not only formally introducing the SGL-SVM but also developing an efficient distributed algorithm to facilitate its application in practical MIR scenarios such as music genre classification, emotion recognition, and auto-tagging.

2.2 Some extensions for CR-SVMs

We introduce two symbols. Specifically, \mathbf{I}_n is the n -dimensional identity matrix, and \mathbf{F} is a $(p-1) \times p$ matrix with all elements being 0, except for 1 on the diagonal and -1 on the superdiagonal. Then three CRTs can be summarized in Table 1.

Table 1: Summarization of three CRTs

Name	Formula	Advantages
EN	$\lambda_1 \ \boldsymbol{\beta}\ _1 + \lambda_2 \ \mathbf{I}_n \boldsymbol{\beta}\ _2^2$	Suitable for highly relevant data
SFL	$\lambda_1 \ \boldsymbol{\beta}\ _1 + \lambda_2 \ \mathbf{F} \boldsymbol{\beta}\ _1$	Suitable for blocky data
SGL	$\lambda_1 \ \boldsymbol{\beta}\ _1 + \lambda_2 \ \mathbf{I}_n \boldsymbol{\beta}\ _{2,1}$	Suitable for grouped data

Obviously, EN, SFL and SGL regularization terms can both be expressed as a linear combination of the ℓ_1 norm and other regularization terms. This structure requires these CRTs to rely on the ℓ_1 norm to achieve sparsity. However, numerous studies, such as those by [Fan and Li \(2001\)](#) and [Zou \(2006\)](#), have confirmed that while the ℓ_1 norm can induce sparsity, it introduces non-negligible estimation bias because it applies the same penalty to all terms. To address the issue of estimation bias caused by the ℓ_1 norm, we consider a non-convex extension of the CRTs. Non-convex regularization terms have a more flexible penalty mechanism. They can achieve sparsity while reducing the over-shrinkage of parameters, thereby reducing the estimation bias. Among these non-convex regularization terms, the most well-known ones are SCAD ([Fan and Li \(2001\)](#)) and MCP ([Zhang \(2010\)](#)), which are summarized in Table 2.

Table 2: The SCAD and MCP

Name	Formula
SCAD ($a > 2$)	$P_{\lambda_1}(\boldsymbol{\beta}_j) = \begin{cases} \lambda_1 \boldsymbol{\beta}_j , & \text{if } \boldsymbol{\beta}_j \leq \lambda_1 \\ \frac{-\boldsymbol{\beta}_j^2 + 2a\lambda_1 \boldsymbol{\beta}_j - \lambda_1^2}{2(a-1)}, & \text{if } \lambda_1 < \boldsymbol{\beta}_j \leq a\lambda_1 \\ \frac{(a+1)\lambda_1^2}{2}, & \text{if } \boldsymbol{\beta}_j > a\lambda_1 \end{cases}$
MCP ($a > 0$)	$P_{\lambda_1}(\boldsymbol{\beta}_j) = \begin{cases} \lambda_1 \boldsymbol{\beta}_j - \frac{\boldsymbol{\beta}_j^2}{2a}, & \text{if } \boldsymbol{\beta}_j \leq a\lambda_1 \\ \frac{a\lambda_1^2}{2}, & \text{if } \boldsymbol{\beta}_j > a\lambda_1 \end{cases}$

Both the SCAD and MCP are defined as the following piecewise function. Such a piecewise design allows for dividing the parameter values into different intervals according to the size of the parameters, and different penalty strategies are adopted in different intervals to reduce the estimation bias. After introducing SCAD and MCP into CRTs, CRTs can be expressed as

$$P_{\lambda_1}(|\boldsymbol{\beta}|) + P_{\lambda_2}(\mathbf{G}\boldsymbol{\beta}), \tag{2.3}$$

where \mathbf{G} is a matrix that changes with the CRTs. For EN and SGL regularization, \mathbf{G} is the n -dimensional identity matrix, and for SFL regularization \mathbf{I}_n , \mathbf{G} is \mathbf{F} .

Another notable extension of CR-SVMs is the loss function. In the traditional SVM model, the hinge loss is a commonly used loss function, which can effectively handle classification problems. However, apart from the hinge loss, there are also some other loss functions that have been applied to the SVM models, such as least squares loss (Langone et al. (2015) and Liang et al. (2024)), huberized hinge loss (Wang et al. (2008)), squared hinge loss (Yang and Zou (2013)), pinball loss (Wang and Xu (2021) and Zhang et al. (2021)) and huberized pinball loss (Zhu et al. (2020)). These losses play a non-negligible role in expanding the application scope of SVM model. The work in Liang et al. (2024) provided a detailed introduction to this, so we will not elaborate further here.

Let $\mathbf{1}_n$ represent n -dimensional vector whose elements are all 1, and \mathbf{Y} be a diagonal matrix with its diagonal elements to be the vector \mathbf{y} . Take $\bar{\mathbf{X}} = \mathbf{Y}\mathbf{X}$, the loss functions can be express as

$$\frac{1}{n} \sum_{i=1}^n L[1 - y_i(\sum_{j=1}^p x_{ij}\beta_j + \beta_0)] = \mathcal{L}(\mathbf{1}_n - \bar{\mathbf{X}}\boldsymbol{\beta} - \mathbf{y}\beta_0) \quad (2.4)$$

where $L : \mathbb{R} \rightarrow [0, \infty)$ is a loss function such as hinge loss, least squares loss, huberized hinge loss, squared hinge loss, pinball loss and huberized pinball loss.

After comprehensively considering the extensions of the CRTs and the loss functions, we can obtain a *unified optimization form* for the CR-SVM models.

$$\min_{\boldsymbol{\beta}, \beta_0} \mathcal{L}(\mathbf{1}_n - \bar{\mathbf{X}}\boldsymbol{\beta} - \mathbf{y}\beta_0) + P_{\lambda_1}(|\boldsymbol{\beta}|) + P_{\lambda_2}(\mathbf{G}\boldsymbol{\beta}). \quad (2.5)$$

This *unified optimization form* is highly versatile and can encompass 54 different types of CR-SVM models (six loss functions in Table 4 multiplied by nine combinations of regularization terms in Table 6). These models differ in the selection of regularization terms and loss functions, and can adapt to different datasets and problem scenarios. Our subsequent algorithm design will be based on this unified framework. That is to say, the algorithm we proposed is highly versatile and effective, and can efficiently solve these 54 CR-SVM models. In this way, we can provide more flexible and accurate solutions for different practical problems and promote the application of SVM models in more fields.

3 Parallel ADMM algorithm for CR-SVMs

In modern data-driven applications, data is often stored in a distributed fashion across multiple machines or nodes due to its large-scale and high-dimensional nature. This distributed storage pattern brings both opportunities and challenges for the design and implementation of machine learning algorithms. When dealing with the CR-SVMs, the distributed storage of data necessitates a new perspective on algorithm design.

Specifically, the original dataset $\{\mathbf{X}, \mathbf{y}\} = \{(\mathbf{x}_i, y_i)\}_{i=1}^n$ is partitioned into K non-overlapping blocks in the context of distributed storage and stored on K machines. Each machine k only has access to its local data $\{\mathbf{X}_k, \mathbf{y}_k\}$ and hence local loss function $\mathcal{L}(\mathbf{1}_k - \bar{\mathbf{X}}_k\boldsymbol{\beta}_k - \mathbf{y}_k\beta_0)$ and the regularization $P_{\lambda_1}(|\boldsymbol{\beta}|) + P_{\lambda_2}(\mathbf{G}\boldsymbol{\beta})$. Then the formula (2.5) can be rewritten as

$$\min_{\{\boldsymbol{\beta}_k\}_{k=1}^K, \boldsymbol{\beta}, \beta_0} \sum_{k=1}^K \mathcal{L}(\mathbf{1}_k - \bar{\mathbf{X}}_k\boldsymbol{\beta}_k - \mathbf{y}_k\beta_0) + P_{\lambda_1}(|\boldsymbol{\beta}|) + P_{\lambda_2}(\mathbf{G}\boldsymbol{\beta}). \quad (3.1)$$

where $\boldsymbol{\beta}_k \in \mathbb{R}^p$, $\bar{\mathbf{X}}_k \in \mathbb{R}^{n_k \times p}$, $\mathbf{1}_k \in \mathbb{R}^{n_k}$, $\mathbf{y}_k \in \mathbb{R}^{n_k}$, and $\sum_{k=1}^K n_k = n$.

In this section, we aim to addressing (3.1) through a parallel algorithm based on the consensus ADMM, which was first introduced by Boyd et al. (2010). Then, we present the implementation process of this algorithm in detail and discuss its time complexity and algorithm convergence.

3.1 Parallel ADMM algorithm for CR-SVMs

To deal with the non-differentiability of the loss function and the non-separability of the CRTs, we introduced additional auxiliary variables $\boldsymbol{\theta}$ ($\in \mathbb{R}^p$ for EN and SGL; $\in \mathbb{R}^{p-1}$ for SFL), $\boldsymbol{\xi}_k \in \mathbb{R}^{n_k}$, $k = 1, 2, \dots, K$ and reformulate problem (3.1) into an equivalent form:

$$\begin{aligned} \min_{\{\boldsymbol{\beta}_k\}_{k=1}^K, \boldsymbol{\theta}, \{\boldsymbol{\xi}_k\}_{k=1}^K, \boldsymbol{\beta}, \beta_0} & \sum_{k=1}^K \mathcal{L}(\boldsymbol{\xi}_k) + P_{\lambda_1}(|\boldsymbol{\beta}|) + P_{\lambda_2}(\boldsymbol{\theta}) \\ \text{s.t.} & \quad \boldsymbol{\xi}_k = \mathbf{1}_k - \bar{\mathbf{X}}_k \boldsymbol{\beta}_k - \mathbf{y}_k \beta_0, \quad k = 1, 2, \dots, K; \\ & \quad \boldsymbol{\beta}_k = \boldsymbol{\beta}, \quad k = 1, 2, \dots, K; \\ & \quad \boldsymbol{\theta} = \mathbf{G}\boldsymbol{\beta} \end{aligned} \quad (3.2)$$

The corresponding augmented Lagrangian function of (3.2) is

$$\begin{aligned} L_\mu(\boldsymbol{\beta}_k, \boldsymbol{\theta}, \boldsymbol{\xi}_k, \boldsymbol{\beta}, \beta_0, \mathbf{b}_k, \mathbf{d}_k, \mathbf{e}) &= \sum_{k=1}^K \mathcal{L}(\boldsymbol{\xi}_k) + P_{\lambda_1}(|\boldsymbol{\beta}|) + P_{\lambda_2}(\boldsymbol{\theta}) - \sum_{k=1}^K \langle \mathbf{b}_k, \boldsymbol{\xi}_k - \mathbf{1}_k + \bar{\mathbf{X}}_k \boldsymbol{\beta}_k + \mathbf{y}_k \beta_0 \rangle \\ &\quad - \sum_{k=1}^K \langle \mathbf{d}_k, \boldsymbol{\beta}_k - \boldsymbol{\beta} \rangle - \langle \mathbf{e}, \boldsymbol{\theta} - \mathbf{G}\boldsymbol{\beta} \rangle + \frac{\mu}{2} \sum_{k=1}^K \|\boldsymbol{\xi}_k - \mathbf{1}_k + \bar{\mathbf{X}}_k \boldsymbol{\beta}_k + \mathbf{y}_k \beta_0\|_2^2 \\ &\quad + \frac{\mu}{2} \sum_{k=1}^K \|\boldsymbol{\beta}_k - \boldsymbol{\beta}\|_2^2 + \frac{\mu}{2} \|\boldsymbol{\theta} - \mathbf{G}\boldsymbol{\beta}\|_2^2 \end{aligned}$$

where $\mathbf{b}_k, \mathbf{d}_k, \mathbf{e}$ are dual variables corresponding to the linear constraints of (3.2), $\mu > 0$ is a tunable augmentation parameter, and $\langle \cdot \rangle$ represents the standard inner product in Euclidean space.

After giving the initial values $(\boldsymbol{\beta}^0, \beta_0^0, \boldsymbol{\theta}^0, \boldsymbol{\xi}_k^0, \boldsymbol{\beta}_k^0, \mathbf{b}_k^0, \mathbf{d}_k^0, \mathbf{e}^0)$, the iterative process of the parallel ADMM can be expressed as

$$\boldsymbol{\beta}_k^{t+1} \leftarrow \arg \min_{\boldsymbol{\beta}_k} L_\mu(\boldsymbol{\beta}_k, \boldsymbol{\theta}^t, \boldsymbol{\xi}_k^t, \boldsymbol{\beta}^t, \beta_0^t, \mathbf{b}_k^t, \mathbf{d}_k^t, \mathbf{e}^t), \quad k = 1, 2, \dots, K \quad (3.3a)$$

$$\boldsymbol{\theta}^{t+1} \leftarrow \arg \min_{\boldsymbol{\theta}} L_\mu(\boldsymbol{\beta}_k^{t+1}, \boldsymbol{\theta}, \boldsymbol{\xi}_k^t, \boldsymbol{\beta}^t, \beta_0^t, \mathbf{b}_k^t, \mathbf{d}_k^t, \mathbf{e}^t) \quad (3.3b)$$

$$\boldsymbol{\xi}_k^{t+1} \leftarrow \arg \min_{\boldsymbol{\xi}_k} L_\mu(\boldsymbol{\beta}_k^{t+1}, \boldsymbol{\theta}^{t+1}, \boldsymbol{\xi}_k, \boldsymbol{\beta}^t, \beta_0^t, \mathbf{b}_k^t, \mathbf{d}_k^t, \mathbf{e}^t), \quad k = 1, 2, \dots, K \quad (3.3c)$$

$$\boldsymbol{\beta}^{t+1} \leftarrow \arg \min_{\boldsymbol{\beta}} L_\mu(\boldsymbol{\beta}_k^{t+1}, \boldsymbol{\theta}^{t+1}, \boldsymbol{\xi}_k^{t+1}, \boldsymbol{\beta}, \beta_0^t, \mathbf{b}_k^t, \mathbf{d}_k^t, \mathbf{e}^t) \quad (3.3d)$$

$$\beta_0^{t+1} \leftarrow \arg \min_{\beta_0} L_\mu(\boldsymbol{\beta}_k^{t+1}, \boldsymbol{\theta}^{t+1}, \boldsymbol{\xi}_k^{t+1}, \boldsymbol{\beta}^{t+1}, \beta_0, \mathbf{b}_k^t, \mathbf{d}_k^t, \mathbf{e}^t) \quad (3.3e)$$

$$\mathbf{b}_k^{t+1} \leftarrow \mathbf{b}_k^t - \mu(\boldsymbol{\xi}_k^{t+1} - \mathbf{1}_k + \bar{\mathbf{X}}_k \boldsymbol{\beta}_k^{t+1} + \mathbf{y}_k \beta_0^{t+1}), \quad k = 1, 2, \dots, K \quad (3.3f)$$

$$\mathbf{d}_k^{t+1} \leftarrow \mathbf{d}_k^t - \mu(\boldsymbol{\beta}_k^{t+1} - \boldsymbol{\beta}^{t+1}), \quad k = 1, 2, \dots, K \quad (3.3g)$$

$$\mathbf{e}^{t+1} \leftarrow \mathbf{e}^t - \mu(\boldsymbol{\theta}^{t+1} - \mathbf{G}\boldsymbol{\beta}^{t+1}) \quad (3.3h)$$

To save time, the iterative process for implementing β_k^{t+1} in (3.3a), ξ_k^{t+1} in (3.3c), \mathbf{b}_k^{t+1} in (3.3f), and \mathbf{d}_k^{t+1} in (3.3g) is parallelized. Next, we will provide detailed closed-form solutions for each subproblem in the iterative process.

3.1.1 For the problem (3.3a)

Regarding the update of β_k^{t+1} , $k = 1, 2, \dots, K$, after rearranging the terms in (3.3a) and omitting constant terms, it can be expressed as:

$$\beta_k^{t+1} \leftarrow \arg \min_{\beta_k} \left\{ \frac{\mu}{2} \sum_{k=1}^K \left\| \xi_k^t - \mathbf{1}_k + \bar{\mathbf{X}}_k \beta_k + \mathbf{y}_k \beta_0^t - \frac{\mathbf{b}_k^t}{\mu} \right\|_2^2 + \frac{\mu}{2} \sum_{k=1}^K \left\| \beta_k - \beta^t - \frac{\mathbf{d}_k^t}{\mu} \right\|_2^2 \right\}. \quad (3.4)$$

This problem is quadratic and differentiable, and we can directly obtain its result by taking the derivative.

$$\beta_k^{t+1} \leftarrow (\bar{\mathbf{X}}_k^T \bar{\mathbf{X}}_k + \mathbf{I}_p)^{-1} \left[\bar{\mathbf{X}}_k^T (-\xi_k^t + \mathbf{1}_k - \mathbf{y}_k \beta_0^t + \frac{\mathbf{b}_k^t}{\mu}) + \beta^t + \frac{\mathbf{d}_k^t}{\mu} \right]. \quad (3.5)$$

When p exceeds n_k , Wu et al. (2025c) proposed applying the Woodbury matrix identity: $(\bar{\mathbf{X}}_k^T \bar{\mathbf{X}}_k + \mathbf{I}_p)^{-1} = \mathbf{I}_p - \bar{\mathbf{X}}_k^T (\mathbf{I}_{n_k} + \bar{\mathbf{X}}_k \bar{\mathbf{X}}_k^T)^{-1} \bar{\mathbf{X}}_k$. This approach proves to be highly practical when the value of n_k is small. The reason is that during the entire ADMM iteration, the inverse matrix only needs to be calculated once. Nevertheless, when both n_k and p are large, computing the inverse matrix can be extremely time-consuming. In such circumstances, the conjugate gradient method introduced in Saad (2003) demonstrates better performance in solving the equation in (3.4). The conjugate gradient method is an efficient iterative algorithm specifically designed for solving symmetric positive definite linear systems of equations. It also shows distinct advantages when dealing with large-scale sparse problems.

3.1.2 For the problem (3.3b)

Regarding the update of θ^{t+1} , after rearranging the terms in (3.3b) and omitting constant terms, it can be expressed as:

$$\theta^{t+1} \leftarrow \arg \min_{\theta} \left\{ P_{\lambda_2}(\theta) + \frac{\mu}{2} \left\| \theta - \mathbf{G} \beta^t - \frac{\mathbf{e}^t}{\mu} \right\|_2^2 \right\}. \quad (3.6)$$

The result of (3.6) depends on $P_{\lambda_2}(\theta)$ and \mathbf{G} , both of which are determined by CRTs. Therefore, we will discuss the specific updated results of θ according to different CRTs.

- For the EN regularization, $P_{\lambda_2}(\theta) = \lambda_2 \|\theta\|_2^2$ and $\mathbf{G} = \mathbf{I}_n$. Formula (3.6) can be expressed as

$$\theta^{t+1} \leftarrow \arg \min_{\theta} \left\{ \lambda_2 \|\theta\|_2^2 + \frac{\mu}{2} \left\| \theta - \beta^t - \frac{\mathbf{e}^t}{\mu} \right\|_2^2 \right\}. \quad (3.7)$$

The minimization problem is quadratic and differentiable, allowing us to solve the subproblem by solving the following linear equations,

$$\theta^{t+1} \leftarrow \frac{\mu(\beta^t + \mathbf{e}^t/\mu)}{2\lambda_2 + \mu}. \quad (3.8)$$

- For the SFL regularization, $P_{\lambda_2}(\boldsymbol{\theta}) = \lambda_2 \|\boldsymbol{\theta}\|_1$ and $\mathbf{G} = \mathbf{F}$. Formula (3.6) can be express as

$$\boldsymbol{\theta}^{t+1} \leftarrow \arg \min_{\boldsymbol{\theta}} \left\{ \lambda_2 \|\boldsymbol{\theta}\|_1 + \frac{\mu}{2} \left\| \boldsymbol{\theta} - \mathbf{F}\boldsymbol{\beta}^t - \frac{\mathbf{e}^t}{\mu} \right\|_2^2 \right\}. \quad (3.9)$$

This is a soft-thresholding operator, and we can directly present the result.

$$\boldsymbol{\theta}^{t+1} \leftarrow \text{Shrink} \left[\mathbf{F}\boldsymbol{\beta}^t + \frac{\mathbf{e}^t}{\mu}, \frac{\lambda_2}{\mu} \right]. \quad (3.10)$$

- For the SGL regularization, $P_{\lambda_2}(\boldsymbol{\theta}) = \lambda_2 \|\boldsymbol{\theta}\|_{2,1}$ and $\mathbf{G} = \mathbf{I}_n$. Formula (3.6) can be express as

$$\boldsymbol{\theta}^{t+1} \leftarrow \arg \min_{\boldsymbol{\theta}} \left\{ \lambda_2 \|\boldsymbol{\theta}\|_{2,1} + \frac{\mu}{2} \left\| \boldsymbol{\theta} - \boldsymbol{\beta}^t - \frac{\mathbf{e}^t}{\mu} \right\|_2^2 \right\}. \quad (3.11)$$

By recalling the definition of the $\ell_{2,1}$ norm ($\|\boldsymbol{\theta}\|_{2,1} = \sum_{m=1}^M \|\boldsymbol{\theta}_{(m)}\|_2$), we can find that $\boldsymbol{\theta}$ is divided into M groups. Since the whole equation (3.11) is separable, the above formula can be regarded as the sum of M ℓ_2 norm proximal operators, which is defined as $\text{prox}_{s,\lambda\|\boldsymbol{\theta}\|_{2,1}}(\mathbf{x}) = \arg \min_{\boldsymbol{\theta}} \{ \lambda \|\boldsymbol{\theta}\|_{2,1} + s/2 \|\boldsymbol{\theta} - \mathbf{x}\|_2^2 \}$. The closed-form solution for $\text{prox}_{s,\lambda\|\boldsymbol{\theta}\|_{2,1}}$ was first presented by Yuan and Lin (2006) and can be expressed as

$$\text{prox}_{s,\lambda\|\boldsymbol{\theta}\|_{2,1}}(\mathbf{x}) = \frac{\mathbf{x}}{\|\mathbf{x}\|_2} \cdot \left[\|\mathbf{x}\|_2 - \frac{\lambda}{s} \right]_+.$$

Then, we have

$$\boldsymbol{\theta}_{(m)}^{t+1} \leftarrow \frac{\boldsymbol{\beta}_{(m)}^t + \frac{\mathbf{e}_{(m)}^t}{\mu}}{\|\boldsymbol{\beta}_{(m)}^t + \frac{\mathbf{e}_{(m)}^t}{\mu}\|_2} \cdot \left[\left\| \boldsymbol{\beta}_{(m)}^t + \frac{\mathbf{e}_{(m)}^t}{\mu} \right\|_2 - \frac{\lambda_2}{\mu} \right]_+, m = 1, 2, \dots, M. \quad (3.12)$$

For convenience, we summarize the updates of $\boldsymbol{\theta}$ under different regularization terms in Table 3.

Table 3: The updated results of $\boldsymbol{\theta}^{t+1}$ under the different CRTs

CRT	The updated result of $\boldsymbol{\theta}^{t+1}$
EN	$\boldsymbol{\theta}^{t+1} \leftarrow \frac{\mu(\boldsymbol{\beta}^t + \mathbf{e}^t/\mu)}{2\lambda_2 + \mu}$
SFL	$\boldsymbol{\theta}^{t+1} \leftarrow \text{Shrink} \left[\mathbf{F}\boldsymbol{\beta}^t + \frac{\mathbf{e}^t}{\mu}, \frac{\lambda_2}{\mu} \right]$
SGL	$\boldsymbol{\theta}_{(m)}^{t+1} \leftarrow \frac{\boldsymbol{\beta}_{(m)}^t + \frac{\mathbf{e}_{(m)}^t}{\mu}}{\ \boldsymbol{\beta}_{(m)}^t + \frac{\mathbf{e}_{(m)}^t}{\mu}\ _2} \cdot \left[\left\ \boldsymbol{\beta}_{(m)}^t + \frac{\mathbf{e}_{(m)}^t}{\mu} \right\ _2 - \frac{\lambda_2}{\mu} \right]_+, m = 1, 2, \dots, M$

3.1.3 For the problem (3.3c)

Regarding the update of $\boldsymbol{\xi}_k^{t+1}, k = 1, 2, \dots, K$, after rearranging the terms in (3.3c) and omitting constant terms, it can be expresses as:

$$\boldsymbol{\xi}_k^{t+1} \leftarrow \arg \min_{\boldsymbol{\xi}} \left\{ \sum_{k=1}^K \left[\mathcal{L}(\boldsymbol{\xi}_k) + \frac{\mu}{2} \left\| \boldsymbol{\xi}_k - \mathbf{1}_k + \bar{\mathbf{X}}_k \boldsymbol{\beta}_k^{t+1} + \mathbf{y}_k \boldsymbol{\beta}_0^t - \frac{\mathbf{b}_k^t}{\mu} \right\|_2^2 \right] \right\}. \quad (3.13)$$

where $\mathcal{L}(\boldsymbol{\xi}_k) = \frac{1}{n_k} \sum_{i=1}^{n_k} L(\xi_{ki})$ is separable. Then the problem (3.13) can be expressed in the form of components.

$$\xi_i^{t+1} \leftarrow \arg \min_{\xi_i} \left\{ \sum_{i=1}^n \left[\frac{1}{n} L(\xi_i) + \frac{\mu}{2} (\xi_i - 1 + y_i (\sum_{j=1}^p x_{ij} \beta_j^{t+1} + \beta_0^t) - \frac{b_i^t}{\mu})^2 \right] \right\}. \quad (3.14)$$

Obviously, the problem (3.14) can be separated into n proximal operators, which is defined as $\text{prox}_{s,L}(x) = \arg \min_{\xi} \{ \frac{1}{n} L(\xi) + s/2(\xi - x)^2 \}$. And its closed-form solution will vary with the change of L , that is, the loss function.

In this paper, we consider six loss functions, namely least squares loss, hinge loss, huberized hinge loss, squared hinge loss, pinball loss and huberized pinball loss. The closed-form solutions of the proximal operators for these six loss functions have been fully discussed in Table 1 of Liang et al. (2024). We will not elaborate on them here but directly present the closed-form solution of equation (3.13) in Table 6 in the form of components. For the convenience of expression, we introduce the symbol $\zeta_i^{t+1} = 1 - y_i (\sum_{j=1}^p x_{ij} \beta_j^{t+1} + \beta_0^t) + \frac{b_i^t}{\mu}$.

Table 4: The closed-form solutions of (3.13) under different loss functions

Loss function	Closed-form solutions of (3.13)
Hinge	$\xi_i^{t+1} = \max\{\zeta_i^{t+1} - \frac{1}{n\mu}, \min(0, \zeta_i^{t+1})\}$
Least square	$\xi_i^{t+1} = \begin{cases} \frac{n\mu\zeta_i^{t+1}}{n\mu+2\zeta_i^{t+1}}, & \zeta_i^{t+1} \geq 0; \\ \frac{n\mu\zeta_i^{t+1}}{n\mu+2(1-\tau)}, & \zeta_i^{t+1} < 0. \end{cases}$
Square hinge	$\xi_i^{t+1} = \begin{cases} \frac{n\mu\zeta_i^{t+1}}{n\mu+1}, & \zeta_i^{t+1} \geq 0; \\ \zeta_i^{t+1}, & \zeta_i^{t+1} < 0. \end{cases}$
Huberized hinge	$\xi_i^{t+1} = \max\{\zeta_i^{t+1} - \frac{1}{n\mu}, \min(\zeta_i^{t+1}, \frac{n\delta\mu\zeta_i^{t+1}}{1+n\delta\mu})\}$
Pinball	$\xi_i^{t+1} = \max\{\zeta_i^{t+1} - \frac{1}{n\mu}, \min(0, \zeta_i^{t+1} + \frac{\tau}{n\mu})\}$
Huberized pinball	$\xi_i^{t+1} = \begin{cases} \frac{n\mu\delta\zeta_i^{t+1}}{n\mu\delta+1} + \frac{1}{n\mu} \left(\frac{n\mu\delta\zeta_i^{t+1}}{n\mu\delta+1} - 1 \right) I(\zeta_i^{t+1} > \frac{1}{n\mu} + \delta), & \zeta_i^{t+1} > 0; \\ \frac{n\mu\delta\zeta_i^{t+1}}{n\mu\delta+\tau} + \frac{\tau}{n\mu} \left(\frac{n\mu\delta\zeta_i^{t+1}}{n\mu\delta+\tau} + 1 \right) I(\zeta_i^{t+1} \leq -\frac{\tau}{n\mu} - \delta), & \zeta_i^{t+1} \leq 0. \end{cases}$

3.1.4 For the problem (3.3d)

Regarding the update of $\boldsymbol{\beta}^{t+1}$, after rearranging the terms in (3.3d) and omitting constant terms, it can be expressed as:

$$\boldsymbol{\beta}^{t+1} \leftarrow \arg \min_{\boldsymbol{\beta}} \left\{ P_{\lambda_1}(|\boldsymbol{\beta}|) + \frac{\mu}{2} \sum_{k=1}^K \|\boldsymbol{\beta}_k^{t+1} - \boldsymbol{\beta} - \frac{\mathbf{d}_k^t}{\mu}\|_2^2 + \frac{\mu}{2} \|\boldsymbol{\theta}^{t+1} - \mathbf{G}\boldsymbol{\beta} - \frac{\mathbf{e}^t}{\mu}\|_2^2 \right\} \quad (3.15)$$

Evidently, the specific result of the above formula hinges on the selection of $P_{\lambda_1}(|\boldsymbol{\beta}|)$ and \mathbf{G} . Next, we will conduct a case-by-case discussion.

- When $P_{\lambda_1}(|\boldsymbol{\beta}|) = \lambda_1 \|\boldsymbol{\beta}\|_1$ and $\mathbf{G} = \mathbf{I}_n$, we rearrange the optimization equation and eliminate certain constant terms that have no bearing on the optimization target variable $\boldsymbol{\beta}$, then the subsequent equation can be derived.

$$\boldsymbol{\beta}^{t+1} \leftarrow \left\{ \arg \min_{\boldsymbol{\beta}} \lambda_1 \|\boldsymbol{\beta}\|_1 + \frac{\mu(K+1)}{2} \|\boldsymbol{\beta}\|^2 - \frac{K(\bar{\boldsymbol{\beta}}^{t+1} - \bar{\mathbf{d}}^t/\mu) + \boldsymbol{\theta}^{t+1} - \mathbf{e}^t/\mu}{K+1} \right\} \quad (3.16)$$

where $\bar{\boldsymbol{\beta}}^{t+1} = K^{-1} \sum_{k=1}^K \boldsymbol{\beta}_k^{t+1}$ and $\bar{\mathbf{d}}^t = K^{-1} \sum_{k=1}^K \mathbf{d}_k^t$. Evidently, the above optimization problem (3.16) corresponds to a soft-thresholding operator, and we can directly obtain the result.

$$\boldsymbol{\beta}^{t+1} \leftarrow \text{Shrink} \left[\frac{K(\bar{\boldsymbol{\beta}}^{t+1} - \bar{\mathbf{d}}^t/\mu) + \boldsymbol{\theta}^{t+1} - \mathbf{e}^t/\mu}{K+1}, \frac{\lambda_1}{\mu K+1} \right] \quad (3.17)$$

where $\text{Shrink}[a, b] = \text{sign}(a) \max\{|a| - b, 0\}$.

- When $P_{\lambda_1}(|\boldsymbol{\beta}|) = \lambda_1 \|\boldsymbol{\beta}\|_1$ and $\mathbf{G} = \mathbf{F}$, we rearrange the optimization equation and eliminate certain constant terms that have no bearing on the optimization target variable $\boldsymbol{\beta}$, then the subsequent equation can be derived.

$$\boldsymbol{\beta}^{t+1} \leftarrow \left\{ \arg \min_{\boldsymbol{\beta}} \lambda_1 \|\boldsymbol{\beta}\|_1 + \frac{\mu}{2} \boldsymbol{\beta}^T (K\mathbf{I}_p + \mathbf{F}^T \mathbf{F}) \boldsymbol{\beta} - \mu \boldsymbol{\beta}^T \left[K(\bar{\boldsymbol{\beta}}^{t+1} - \frac{\bar{\mathbf{d}}^t}{\mu}) + \mathbf{F}^T (\boldsymbol{\theta}^{t+1} - \frac{\mathbf{e}^t}{\mu}) \right] \right\} \quad (3.18)$$

It is quite evident that, owing to the non-identity matrix preceding the quadratic term of $\boldsymbol{\beta}$ and the presence of $\|\boldsymbol{\beta}\|_1$, Equation (3.18) does not possess a closed-form solution. While numerical approaches like the coordinate descent method can be employed to solve (3.18), this would substantially elevate the computational load. In this context, we put forward the use of a linearization technique to approximate this optimization problem and acquire a closed-form solution for the problem (3.18).

We can linearize the quadratic term $\frac{\mu}{2} \boldsymbol{\beta}^T (K\mathbf{I}_p + \mathbf{F}^T \mathbf{F}) \boldsymbol{\beta} - \mu \boldsymbol{\beta}^T \left[K(\bar{\boldsymbol{\beta}}^{t+1} - \frac{\bar{\mathbf{d}}^t}{\mu}) + \mathbf{F}^T (\boldsymbol{\theta}^{t+1} - \frac{\mathbf{e}^t}{\mu}) \right]$ in (3.18) and replace it by

$$\left\{ \mu (K\mathbf{I}_p + \mathbf{F}^T \mathbf{F})^T \boldsymbol{\beta}^t - \mu \left[K(\bar{\boldsymbol{\beta}}^{t+1} - \frac{\bar{\mathbf{d}}^t}{\mu}) + \mathbf{F}^T (\boldsymbol{\theta}^{t+1} - \frac{\mathbf{e}^t}{\mu}) \right] \right\} (\boldsymbol{\beta} - \boldsymbol{\beta}^t) + \frac{\eta}{2} \|\boldsymbol{\beta} - \boldsymbol{\beta}^t\|_2^2 \quad (3.19)$$

where the linearization parameter $\eta > 0$ serves to regulate the closeness between $\boldsymbol{\beta}$ and $\boldsymbol{\beta}^t$. To guarantee the convergence of the algorithm, η must exceed the largest eigenvalue of the matrix $(K\mathbf{I}_p + \mathbf{F}^T \mathbf{F})$. It is worth noting, as pointed out by Wu et al. (2025c), that due to the special structure of the matrix \mathbf{F} , the largest eigenvalue of $(K\mathbf{I}_p + \mathbf{F}^T \mathbf{F})$ is exactly $K + 4$. As a result, we can conveniently set $\eta = K + 4.01$. Consequently, we can tackle the following problem

$$\boldsymbol{\beta}^{t+1} \leftarrow \arg \min_{\boldsymbol{\beta}} \left\{ \lambda_1 \|\boldsymbol{\beta}\|_1 + \frac{\eta}{2} \left\| \boldsymbol{\beta} - \boldsymbol{\beta}^t + \frac{\mu}{\eta} \left[(K\mathbf{I}_p + \mathbf{F}^T \mathbf{F}) \boldsymbol{\beta}^t - K(\bar{\boldsymbol{\beta}}^{t+1} - \frac{\bar{\mathbf{d}}^t}{\mu}) - \mathbf{F}^T (\boldsymbol{\theta}^{t+1} - \frac{\mathbf{e}^t}{\mu}) \right] \right\|_2^2 \right\} \quad (3.20)$$

to attain an approximate solution for the (3.18).

$$\boldsymbol{\beta}^{t+1} \leftarrow \text{Shrink} \left[\boldsymbol{\beta}^t - \frac{\mu}{\eta} \left((K\mathbf{I}_p + \mathbf{F}^T \mathbf{F}) \boldsymbol{\beta}^t - K(\bar{\boldsymbol{\beta}}^{t+1} - \frac{\bar{\mathbf{d}}^t}{\mu}) - \mathbf{F}^T (\boldsymbol{\theta}^{t+1} - \frac{\mathbf{e}^t}{\mu}) \right), \frac{\lambda_1}{\eta} \right] \quad (3.21)$$

• When $P_{\lambda_1}(|\boldsymbol{\beta}|) = \text{SCAD}$ or MCP , we need to introduce the local linear approximation (LLA) method proposed by [Zou and Li \(2008\)](#) due to the non-convexity of the SCAD and MCP regularization terms. As stated in [Zou and Li \(2008\)](#), non-convex regularization terms can be approximated as

$$P_{\lambda}(|\beta_j|) \approx P_{\lambda}(|\beta_j^{(0)}|) + P'_{\lambda}(|\beta_j^{(0)}|)(|\beta_j| - |\beta_j^{(0)}|), \text{ for } \beta_j \approx \beta_j^{(0)}, j = 1, 2, \dots, p. \quad (3.22)$$

It should be noted that when using the LLA algorithm to solve non-convex problems, a suitable initial value $\beta_j^{(0)}$ is of great significance. In this paper, we adopt the same approach as [Gu et al. \(2018\)](#). That is, we use the solution of the ℓ_1 regularization problem in (3.2) as the initial value. The specific operational details can be found in [Wu et al. \(2025b\)](#) and [Wu et al. \(2025c\)](#), and the convergence analysis of the corresponding algorithm can be found in [Wu et al. \(2025a\)](#). The results of $P'_{\lambda}(|\beta_j|)$ for different non-convex regularization terms are summarized in the Table 5.

Table 5: The $P'_{\lambda}(|\beta_j|)$ of SCAD and MCP

Name	Formula
SCAD ($a > 2$)	$P'_{\lambda}(\beta_j) = \begin{cases} \lambda_1, & \text{if } \beta_j \leq \lambda_1, \\ \frac{a\lambda_1 - \beta_j }{a-1}, & \text{if } \lambda_1 < \beta_j < a\lambda_1, \\ 0, & \text{if } \beta_j \geq a\lambda_1. \end{cases}$
MCP ($a > 0$)	$P'_{\lambda}(\beta_j) = \begin{cases} \lambda_1 - \frac{ \beta_j }{a}, & \text{if } \beta_j \leq a\lambda_1 \\ 0, & \text{if } \beta_j > a\lambda_1 \end{cases}$

Then, the problem (3.15) can be approximately formulated as

$$\boldsymbol{\beta}^{t+1} \leftarrow \arg \min_{\boldsymbol{\beta}} \left\{ \sum_{j=1}^p P'_{\lambda_1}(|\beta_j^t|)|\beta_j| + \frac{\mu}{2} \sum_{k=1}^K \|\boldsymbol{\beta}_k^{t+1} - \boldsymbol{\beta} - \frac{\mathbf{d}_k^t}{\mu}\|_2^2 + \frac{\mu}{2} \|\boldsymbol{\theta}^{t+1} - \mathbf{G}\boldsymbol{\beta} - \frac{\mathbf{e}^t}{\mu}\|_2^2 \right\}. \quad (3.23)$$

We can observe that, compared with the problem (3.15), the only difference is that the parameter λ in it has been replaced with $P'_{\lambda_1}(|\beta_j^t|)$. This implies that we only need to make minor adjustments to the above results to obtain the result of (3.23).

$$\boldsymbol{\beta}^{t+1} \leftarrow \text{Shrink} \left[\frac{K(\bar{\boldsymbol{\beta}}^{t+1} - \bar{\mathbf{d}}^t/\mu) + \boldsymbol{\theta}^{t+1} - \mathbf{e}^t/\mu}{K+1}, \frac{P'_{\lambda_1}(|\beta_j^t|)}{\mu K + 1} \right], \quad (3.24)$$

$$\boldsymbol{\beta}^{t+1} \leftarrow \text{Shrink} \left[\boldsymbol{\beta}^t - \frac{\mu}{\eta} \left((K\mathbf{I}_p + \mathbf{F}^T \mathbf{F})\boldsymbol{\beta}^t - K(\bar{\boldsymbol{\beta}}^{t+1} - \frac{\bar{\mathbf{d}}^t}{\mu}) - \mathbf{F}^T(\boldsymbol{\theta}^{t+1} - \frac{\mathbf{e}^t}{\mu}) \right), \frac{P'_{\lambda_1}(|\beta_j^t|)}{\eta} \right], \quad (3.25)$$

where the values of each component of $\boldsymbol{\beta}^{t+1} = (\beta_1^{t+1}, \beta_2^{t+1}, \dots, \beta_p^{t+1})^T$ will vary with the value of $P'_{\lambda_1}(|\beta_j^t|), j = 1, 2, \dots, p$. The solutions in (3.24) and (3.25) are for $\mathbf{G} = \mathbf{I}_n$ and $\mathbf{G} = \mathbf{F}$ respectively.

We summarize the updated results of $\boldsymbol{\beta}^{t+1}$ under the different scenarios mentioned above in Table 6.

Table 6: The updated results of β^{t+1} under the different scenarios

	$P_\lambda(\beta) = \ell_1$	$P_\lambda(\beta) = \text{SACD}$	$P_\lambda(\beta) = \text{MCP}$
EN ($G = \mathbf{I}_n$)	(3.17)	(3.24)	(3.24)
SFL ($G = \mathbf{F}$)	(3.21)	(3.25)	(3.25)
SGL ($G = \mathbf{I}_n$)	(3.17)	(3.24)	(3.24)

3.1.5 For the problem (3.3e)

Regarding the update of β_0^{t+1} , after rearranging the terms in (3.3e) and omitting constant terms, it can be expressed as:

$$\beta_0^{t+1} \leftarrow \arg \min_{\beta_0} \left\{ \frac{\mu}{2} \sum_{k=1}^K \left\| \xi_k^{t+1} - \mathbf{1}_k + \bar{\mathbf{X}}_k \beta_k^{t+1} + \mathbf{y}_k \beta_0 - \frac{\mathbf{b}_k^t}{\mu} \right\|_2^2 \right\}. \quad (3.26)$$

This problem is quadratic and differentiable, and we can directly obtain its result,

$$\beta_0^{t+1} \leftarrow \sum_{k=1}^K \frac{1}{n_k} \mathbf{y}_k^T \left(-\xi_k^{t+1} + \mathbf{1}_k - \bar{\mathbf{X}}_k \beta_k^{t+1} + \frac{\mathbf{b}_k^t}{\mu} \right). \quad (3.27)$$

Since the update of β_0^{t+1} requires the data on all local machines, to reduce the communication cost, we calculate

$$c_k^{t+1} = \frac{1}{n_k} \mathbf{y}_k^T \left(-\xi_k^{t+1} + \mathbf{1}_k - \bar{\mathbf{X}}_k \beta_k^{t+1} + \frac{\mathbf{b}_k^t}{\mu} \right), k = 1, 2, \dots, K, \quad (3.28)$$

on each local machine respectively and then aggregate them to the central machine for addition.

3.2 Gaussian Back Substitution

Recall that in formula (3.2), for distributed data storage, Algorithm 1 has a total of $2k + 3$ primal variables, i.e., $\{\beta_k, \theta, \xi_k, \beta, \beta_0\}, k = 1, 2, \dots, K$. Additionally, the constraint matrices related to these primal variables cannot be split into two mutually-orthogonal groups. Hence, Algorithm 1 should be categorized as a multi-block ADMM algorithm. Chen et al. (2016) pointed out that the ADMM algorithm with three or more blocks does not always guarantee convergence unless the constraint coefficient matrices are orthogonal. If the constraint coefficients of all the primal sub-problems can form two orthogonal matrices, the multi-block ADMM algorithm can be transformed into the traditional two-block ADMM algorithm, thus ensuring convergence. However, due to the presence of the intercept term β_0 , the iterations process (3.3) cannot be transformed into a two-block ADMM algorithm, but only into a three-block one.

He et al. (2012) pointed out that for the three-block ADMM algorithm to have a theoretical guarantee of convergence, it is necessary to correct certain iterative solutions. The correction method they proposed involves introducing an upper triangular block matrix. Due to the characteristics of this matrix, this method is known as the *Gaussian back substitution*. This technique is widely applied to ensure the convergence of multi-block ADMM algorithms. For example, Wu et al. (2025b) refined the existing

parallel ADMM algorithms designed to tackle high-dimensional quantile regression and classification problems by implementing the Gaussian back substitution strategy. This refinement effectively guarantees the convergence of these algorithms.

In this paper, we will also employ the Gaussian back substitution method to correct the iterative solutions generated by (3.3), thereby ensuring the convergence of the algorithm. To distinguish between the iterative variables generated by (3.3) and the corrected variables, we denote the $(t + 1)$ -th iterative solutions generated by (3.3) as $\{\tilde{\boldsymbol{\beta}}_k^t, \tilde{\boldsymbol{\theta}}^t, \tilde{\boldsymbol{\xi}}_k^t, \tilde{\boldsymbol{\beta}}^t, \tilde{\beta}_0^t, \tilde{\mathbf{b}}_k^t, \tilde{\mathbf{d}}_k^t, \tilde{\mathbf{e}}^t\}$, $k = 1, 2, \dots, K$ and the corrected ones as $\{\boldsymbol{\beta}_k^{t+1}, \boldsymbol{\theta}^{t+1}, \boldsymbol{\xi}_k^{t+1}, \boldsymbol{\beta}^{t+1}, \beta_0^{t+1}, \mathbf{b}_k^{t+1}, \mathbf{d}_k^{t+1}, \mathbf{e}^{t+1}\}$, $k = 1, 2, \dots, K$.

Let $\mathbf{v}_1 = (\boldsymbol{\beta}_1^\top, \boldsymbol{\beta}_2^\top, \dots, \boldsymbol{\beta}_K^\top, \boldsymbol{\theta}^\top)^\top$, $\mathbf{v}_2 = (\boldsymbol{\xi}_1^\top, \boldsymbol{\xi}_2^\top, \dots, \boldsymbol{\xi}_K^\top)^\top$, $\mathbf{v}_3 = (\boldsymbol{\beta}^\top, \beta_0)^\top$ and $\varphi_1(\mathbf{v}_1) = P_{\lambda_2}(\boldsymbol{\theta})$, $\varphi_2(\mathbf{v}_2) = \sum_{k=1}^K \mathcal{L}(\boldsymbol{\xi}_k)$, $\varphi_3(\mathbf{v}_3) = P_{\lambda_1}(|\boldsymbol{\beta}|)$, the optimization problem (3.2) can be transformed as

$$\begin{aligned} \min_{\mathbf{v}_1, \mathbf{v}_2, \mathbf{v}_3} \quad & \varphi_1(\mathbf{v}_1) + \varphi_2(\mathbf{v}_2) + \varphi_3(\mathbf{v}_3) \\ \text{s.t.} \quad & \mathbf{A}\mathbf{v}_1 + \mathbf{B}\mathbf{v}_2 + \mathbf{C}\mathbf{v}_3 = \mathbf{z}, \end{aligned} \quad (3.29)$$

where $\mathbf{z} = (\mathbf{1}_1^\top, \mathbf{1}_2^\top, \dots, \mathbf{1}_K^\top, \mathbf{0}^\top, \mathbf{0}^\top, \dots, \mathbf{0}^\top, \mathbf{0}^\top)^\top$, the three matrices \mathbf{A} , \mathbf{B} , and \mathbf{C} are defined as follows:

$$\begin{aligned} \mathbf{A} = [\mathbf{A}_1, \mathbf{A}_2, \dots, \mathbf{A}_K, \mathbf{A}_{K+1}] &= \begin{bmatrix} \bar{\mathbf{X}}_1^\top & \mathbf{0}^\top & \dots & \mathbf{0}^\top & \mathbf{I}_p & \mathbf{0}^\top & \dots & \mathbf{0}^\top & \mathbf{0}^\top \\ \mathbf{0}^\top & \bar{\mathbf{X}}_2^\top & \dots & \mathbf{0}^\top & \mathbf{0}^\top & \mathbf{I}_p & \dots & \mathbf{0}^\top & \mathbf{0}^\top \\ \vdots & \vdots & \ddots & \vdots & \vdots & \vdots & \ddots & \vdots & \vdots \\ \mathbf{0}^\top & \mathbf{0}^\top & \dots & \bar{\mathbf{X}}_K^\top & \mathbf{0}^\top & \mathbf{0}^\top & \dots & \mathbf{I}_p & \mathbf{0}^\top \\ \mathbf{0}^\top & \mathbf{0}^\top & \dots & \mathbf{0}^\top & \mathbf{0}^\top & \mathbf{0}^\top & \dots & \mathbf{0}^\top & \mathbf{I}_G \end{bmatrix}_{(K+1) \times (2K+1)} \\ \mathbf{B} = [\mathbf{B}_1, \mathbf{B}_2, \dots, \mathbf{B}_K] &= \begin{bmatrix} \mathbf{I}_{n_1} & \mathbf{0}^\top & \dots & \mathbf{0}^\top & \mathbf{0}^\top & \mathbf{0}^\top & \dots & \mathbf{0}^\top & \mathbf{0}^\top \\ \mathbf{0}^\top & \mathbf{I}_{n_2} & \dots & \mathbf{0}^\top & \mathbf{0}^\top & \mathbf{0}^\top & \dots & \mathbf{0}^\top & \mathbf{0}^\top \\ \vdots & \vdots & \ddots & \vdots & \vdots & \vdots & \ddots & \vdots & \vdots \\ \mathbf{0}^\top & \mathbf{0}^\top & \dots & \mathbf{I}_{n_K} & \mathbf{0}^\top & \mathbf{0}^\top & \dots & \mathbf{0}^\top & \mathbf{0}^\top \end{bmatrix}_{K \times (2K+1)} \\ \mathbf{C} = [\mathbf{C}_1, \mathbf{C}_2] &= \begin{bmatrix} \mathbf{0}^\top & \mathbf{0}^\top & \dots & \mathbf{0}^\top & -\mathbf{I}_p & -\mathbf{I}_p & \dots & -\mathbf{I}_p & -\mathbf{G}^\top \\ \mathbf{y}_1^\top & \mathbf{y}_2^\top & \dots & \mathbf{y}_K^\top & \mathbf{0}^\top & \mathbf{0}^\top & \dots & \mathbf{0}^\top & \mathbf{0}^\top \end{bmatrix}_{2 \times (2K+1)}. \end{aligned}$$

Then, the Gaussian back substitution of $(\mathbf{v}_2^{t+1}, \mathbf{v}_3^{t+1})$ is defined as

$$\begin{bmatrix} \mathbf{v}_2^{t+1} \\ \mathbf{v}_3^{t+1} \end{bmatrix} = \begin{bmatrix} \mathbf{v}_2^t \\ \mathbf{v}_3^t \end{bmatrix} - \begin{bmatrix} \nu \mathbf{I} & -\nu (\mathbf{B}^\top \mathbf{B})^{-1} \mathbf{B}^\top \mathbf{C} \\ \mathbf{0} & \nu \mathbf{I} \end{bmatrix} \begin{bmatrix} \mathbf{v}_2^t - \tilde{\mathbf{v}}_2^t \\ \mathbf{v}_3^t - \tilde{\mathbf{v}}_3^t \end{bmatrix} \quad (3.30)$$

where $\nu \in (0, 1)$. From the definition of the constraint matrix \mathbf{B} , we know that $\mathbf{B}^\top \mathbf{B}$ is an identity matrix. This effectively avoids calculating the inverse of a large-scale matrix and significantly reduces the computational burden. And we have

$$(\mathbf{B}^\top \mathbf{B})^{-1} \mathbf{B}^\top \mathbf{C} = \mathbf{B}^\top \mathbf{C} = \begin{bmatrix} \mathbf{0} & \mathbf{y}_1 \\ \mathbf{0} & \mathbf{y}_2 \\ \vdots & \vdots \\ \mathbf{0} & \mathbf{y}_k \end{bmatrix}.$$

Then according to (3.30), it can be derived

$$\boldsymbol{\xi}_k^{t+1} = (1 - \nu)\boldsymbol{\xi}_k^t + \nu\tilde{\boldsymbol{\xi}}_k^t + \nu\mathbf{y}_k(\beta_0^t - \tilde{\beta}_0^t), k = 1, 2, \dots, K; \quad (3.31a)$$

$$\boldsymbol{\beta}^{t+1} = (1 - \nu)\boldsymbol{\beta}^t + \nu\tilde{\boldsymbol{\beta}}^t, k = 1, 2, \dots, K; \quad (3.31b)$$

$$\beta_0^{t+1} = (1 - \nu)\beta_0^t + \nu\tilde{\beta}_0^t. \quad (3.31c)$$

where $\tilde{\boldsymbol{\xi}}_k^t$, $\tilde{\boldsymbol{\beta}}^t$, and $\tilde{\beta}_0^t$ are generated by (3.3) at the $(t + 1)$ -th iterations. Since there is no need to make corrections to $\tilde{\mathbf{v}}_1^{t+1}$, we have $\boldsymbol{\beta}_k^{t+1} = \tilde{\boldsymbol{\beta}}_k^t$ and $\boldsymbol{\theta}^{t+1} = \tilde{\boldsymbol{\theta}}^t$.

After discussing the updates of each sub-problem and Gaussian back substitution, it can be found that $\boldsymbol{\beta}$, $\boldsymbol{\theta}$ and \mathbf{e} do not require data loading and their updates can be performed on the central machine. However, $\boldsymbol{\xi}_k$, $\boldsymbol{\beta}_k$, \mathbf{b}_k and \mathbf{d}_k need to use the data set, so their updates should be carried out on the local machines. Notably, the update of β_0^{t+1} necessitates data from all local machines. To minimize communication costs, we opt to compute c_k^{t+1} on each individual local machine separately. Subsequently, these computed values are transmitted to the central machine for averaging, ultimately yielding the value of β_0^{t+1} . In addition, since the update of $\boldsymbol{\beta}$ requires $\boldsymbol{\beta}_k$ and \mathbf{d}_k , the local machines need to transmit these two pieces of information to the central machine. And the update of $\boldsymbol{\beta}_k$ and $\boldsymbol{\xi}_k$ on the local machines requires the information of $\boldsymbol{\beta}$ and β_0 , so the central machine needs to transmit the corresponding information to the local machines.

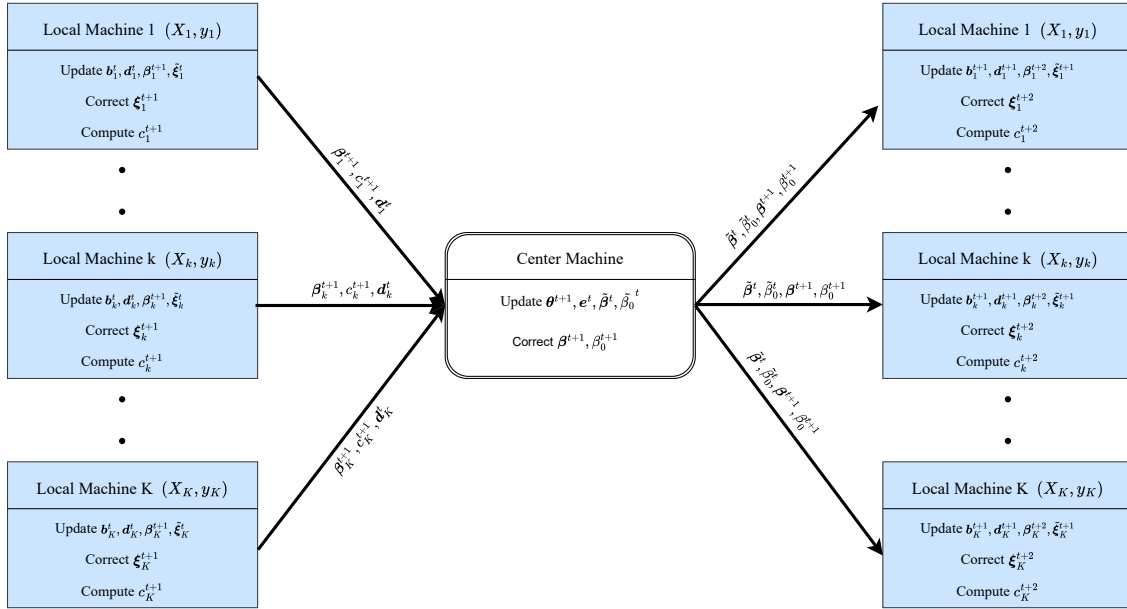


Figure 1: Schematic diagram of the implementation of parallel ADMM algorithm

However, the update sequence ($\boldsymbol{\beta}_k \rightarrow \boldsymbol{\theta} \rightarrow \boldsymbol{\xi}_k \rightarrow \boldsymbol{\beta} \rightarrow \beta_0 \rightarrow \mathbf{b}_k \rightarrow \mathbf{d}_k \rightarrow \mathbf{e}$), specifically designed for the convergence analysis, will lead to inconsistent updates of variables on the local machines. We must first complete the updates of $\boldsymbol{\beta}^{t+1}$ and β_0^{t+1} on the central machine before proceeding with the updates of \mathbf{b}_k^{t+1} and \mathbf{d}_k^{t+1} . This results in an additional round of communication between the central machine and the local machines, thereby reducing the efficiency of the algorithm. Fortunately, the update order of the dual variables has no impact on the accuracy and convergence of the algorithm. Therefore, We opt to

place the dual variables \mathbf{b}_k^t and \mathbf{d}_k^t from the t -th iteration at the starting point of the $(t+1)$ -th iteration for updating. The updated \mathbf{b}_k^t and \mathbf{d}_k^t after adjustment can be expressed as follows

$$\mathbf{b}_k^t = \mathbf{b}_k^{t-1} - \mu(\tilde{\boldsymbol{\xi}}_k^{t-1} - \mathbf{1}_k + \bar{\mathbf{X}}_k \boldsymbol{\beta}_k^t + \mathbf{y}_k \tilde{\beta}_0^{t-1}) \quad (3.32a)$$

$$\mathbf{d}_k^t = \mathbf{d}_k^{t-1} - \mu(\boldsymbol{\beta}_k^t - \tilde{\boldsymbol{\beta}}^{t-1}) \quad (3.32b)$$

Although updating the dual variable \mathbf{e} does not incur additional communication costs, for the sake of algorithmic tidiness, we also choose to adjust \mathbf{e}^t .

$$\mathbf{e}^t = \mathbf{e}^{t-1} - \mu(\boldsymbol{\theta}^t - \mathbf{G}\tilde{\boldsymbol{\beta}}^{t-1}) \quad (3.33)$$

After the aforementioned adjustments, the update sequence of the algorithm has changed to $(\mathbf{b}_k \rightarrow \mathbf{d}_k \rightarrow \boldsymbol{\beta}_k \rightarrow \boldsymbol{\theta} \rightarrow \boldsymbol{\xi}_k \rightarrow \mathbf{e} \rightarrow \boldsymbol{\beta} \rightarrow \beta_0)$. We use Figure 1 to illustrate the specific operations of the proposed algorithm, and the more detailed content of the algorithm is summarized in Algorithm 1.

Algorithm 1 Parallel ADMM for solving the CR-SVMs

Input: • Central machine: $\mu, K, \lambda_1, \lambda_2, \boldsymbol{\beta}^0, \boldsymbol{\theta}^0$ and \mathbf{e}^0 .

• The k -th local machine: $\mathbf{X}_k, \mathbf{y}_k; \mu, \beta_{0k}^0, \boldsymbol{\xi}_k^0, \boldsymbol{\beta}_k^0, b_k^0, \mathbf{d}_k^0$ and selectable parameters $\tau \in (0, 1]$ and $\delta > 0$ for loss function.

Output: the total number of iterations T , $\boldsymbol{\beta}^T$ and β_0^T .

while not converged **do**

Local machines: for $k = 1, 2, \dots, K$ (in parallel)

1. Receive $\tilde{\boldsymbol{\beta}}^{t-1}, \tilde{\beta}_0^{t-1}$ and $\boldsymbol{\beta}^t, \beta_0^t$ transmitted by the central machine,
2. Update \mathbf{b}_k^t by (3.32a) and \mathbf{d}_k^t by (3.32b),
3. Update $\boldsymbol{\beta}_k^{t+1}$ by (3.5),
4. Update $\tilde{\boldsymbol{\xi}}_k^t$ by Table 6 according to different loss functions, then correct $\boldsymbol{\xi}_k^{t+1}$ by (3.31a)
5. Compute c_k by (3.28),
6. Send $c_k, \boldsymbol{\beta}_k^{t+1}$ and \mathbf{d}_k^t to the central machine.

- Central machine:**
1. Receive $\boldsymbol{\beta}_k^{t+1}, \mathbf{d}_k^t$ and c_k^{t+1} transmitted by local machines $k, k = 1, 2, \dots, K$,
 2. Update $\boldsymbol{\theta}^{t+1}$ by Table 5 according to different models,
 3. Update \mathbf{e}^t by (3.33),
 4. Update $\tilde{\boldsymbol{\beta}}^t$ by Table 4 according to different models, then correct $\boldsymbol{\beta}^{t+1}$ by (3.31b),
 5. Update $\tilde{\beta}_0^t$ by adding K c_k , then correct β_0^{t+1} by (3.31c),
 6. Send $\tilde{\boldsymbol{\beta}}^t, \tilde{\beta}_0^t$ and $\boldsymbol{\beta}^{t+1}, \beta_0^{t+1}$ to the local machines.

end while

return solution.

3.3 Convergence and computational cost analysis

The convergence analysis of the three - block ADMM algorithm modified by Gaussian back-substitution has been comprehensively explored, as demonstrated in the works of He et al. (2012) and Wu et al. (2025b), among others. Here, we directly present the convergence conclusion of Algorithm 1. For the detailed proof, please refer to the first section of supporting materials.

Theorem 1 Let $\mathbf{h}^t = (\boldsymbol{\beta}^t, \beta_0^t, \{\boldsymbol{\xi}_k^t\}_{k=1}^K, \{\boldsymbol{\beta}_k^t\}_{k=1}^K, \boldsymbol{\theta}^t, \{\mathbf{b}_k^t\}_{k=1}^K, \{\mathbf{d}_k^t\}_{k=1}^K, \mathbf{e}^t)$ be generated by Algorithm 1 with an initial feasible solution \mathbf{h}^0 . The sequence $\mathbf{g}^t = (\{\boldsymbol{\xi}_k^t\}_{k=1}^K, \boldsymbol{\beta}^t, \beta_0^t, \{\mathbf{b}_k^t\}_{k=1}^K, \{\mathbf{d}_k^t\}_{k=1}^K, \mathbf{e}^t)$ converge to \mathbf{g}^* , where $\mathbf{g}^* = (\{\boldsymbol{\xi}_k^*\}_{k=1}^K, \boldsymbol{\beta}^*, \beta_0^*, \{\mathbf{b}_k^*\}_{k=1}^K, \{\mathbf{d}_k^*\}_{k=1}^K, \mathbf{e}^*)$ is an optimal solution point of (3.1). For any

positive integer $T > 0$, the $O(1/T)$ convergence rate in a non-ergodic sense can also be obtained, i.e.,

$$\|\mathbf{g}^T - \mathbf{g}^{T+1}\|_{\mathbf{H}}^2 \leq \frac{1}{c_0(T+1)} \|\mathbf{g}^0 - \mathbf{g}^*\|_{\mathbf{H}}^2 \quad (3.34)$$

where $c_0 > 0$ is a constant, \mathbf{H} is a positive definite matrix and its specific form can be found in the proof of this theorem.

In the proof of this theorem, we discover that the sequences $\{\|\mathbf{g}^t - \mathbf{g}^*\|_{\mathbf{H}}^2\}$ and $\{\|\mathbf{g}^{t+1} - \mathbf{g}^t\|_{\mathbf{H}}^2\}$ are monotonically non-increasing, and $\sum_{t=0}^{\infty} c_0 \|\mathbf{g}^{t+1} - \mathbf{g}^t\|_{\mathbf{H}}^2 \leq \|\mathbf{g}^0 - \mathbf{g}^*\|_{\mathbf{H}}^2 < +\infty$. From the lemma 1.1 in [Deng et al. \(2013\)](#), we can draw the following conclusion.

Corollary 3.1 *The improved sublinear convergence rate in a non-ergodic sense can be obtained, that is,*

$$\|\mathbf{g}^{t+1} - \mathbf{g}^t\|_{\mathbf{H}}^2 = o(1/t). \quad (3.35)$$

Next, we will provide the complexity of algorithm iteration, which is detailed in the second section of supporting materials.

Theorem 2 *The overall computational complexity of Algorithm 1 is*

$$\begin{cases} O(n_{\max} p^2) + O(n_{\max} p) \times T & \text{If } n_{\max} > p, \\ O(n_{\max}^2 p) + O(p^2) \times T & \text{otherwise,} \end{cases} \quad (3.36)$$

where $n_{\max} = \max\{n_k\}_{k=1}^K$ and T is the total number of iterations in the ADMM algorithm.

This theorem indicates that adding sub-machines can effectively reduce the computational complexity of the algorithm. This is because increasing the number of sub-machines reduces the value of n_{\max} , which is consistent with the conclusion of [Wu et al. \(2025c\)](#). Moreover, this complexity is independent of the loss function and regularization term, demonstrating the universality of algorithm.

4 Numerical results

In this section, we compare the performance of the proposed parallel algorithm and the existing state-of-the-art algorithms in synthetic data and real data. In general, all the parameters (for algorithms) μ , λ_1 and λ_2 need to be chosen by the cross-validation (CV) method, while leading to the high computational burden. To reduce the computational cost, we suggest that μ is selected from the set $\{0.01, 0.1, 1\}$. Moreover, to choose the optimal values for the regularization parameters λ_1, λ_2 , we adopt the method proposed in [Zhang et al. \(2016\)](#), which minimizes the SVM information criterion (SVMIC). SVMIC is defined as:

$$\text{SVMIC}(\boldsymbol{\lambda}) = \sum_{i=1}^n \xi_n + |S_{\lambda_1, \lambda_2}| \log n + 2\gamma \binom{p}{|S_{\lambda_1, \lambda_2}|}. \quad (4.1)$$

Here, $\gamma \in [0, 1]$ and $|S_{\lambda_1, \lambda_2}|$ is the number of non-zero coordinates in estimator. All the experiments in this paper prove that the selection of these parameters is very effective. We put the R codes for implementing

the proposed parallel algorithm and reproducing our experiments on <https://github.com/xfwu1016/PADMM-for-Svms>. The iteration initial values of the prime and dual variables are both set to be $\mathbf{0}$.

In order to accelerate the convergence speed of the proposed parallel algorithm, we adopt the following acceleration method. One is the effective and simple method of adjusting μ proposed by [Boyd et al. \(2010\)](#), that is

$$\mu^{k+1} = \begin{cases} \mu^k * c_2, & \text{if } c_1 \times \text{primal residual} < \text{dual residual}, \\ \mu^k / c_2, & \text{if } \text{primal residual} > c_1 \times \text{dual residual}, \\ \mu^k, & \text{otherwise,} \end{cases} \quad (4.2)$$

where $c_1 = 10, c_2 = 2$, the definitions of the above two residuals can be found in Chapter 3.3 of [Boyd et al. \(2010\)](#). This self-adaptive tuning method has been used by [Boyd et al. \(2010\)](#), and they also claimed that the convergence of ADMM can be guaranteed if μ^k becomes fixed after a finite number of iterations. The proposed MLADMM algorithm is iterated until some stopping criterion is satisfied. We use the stopping criterion from the Chapter 3.3.1 of [Boyd et al. \(2010\)](#). All experiments were conducted on a computer equipped with an AMD Ryzen 9 7950X 16-core processor (clocked at 4.50 GHz) and 32 GB of memory, using the R programming language.

Table 7: Comparison of different Parallrl ADMM algorithms for SVMs

PADMM		$(n, p) = (200000, 500)$				PADMM		$(n, p) = (500000, 1000)$	
K	CAR	CT	NI	NTSF	CAR	CT	NI	NTSF	
5	0.982(0.002)	2.230(0.258)	19.412(1.822)	10.1(0.001)	0.979(0.002)	4.678(0.571)	25.121(2.803)	10.4(0.002)	
10	0.980(0.003)	1.510(0.179)	22.513(2.132)	10.2(0.001)	0.975(0.003)	2.855(0.325)	30.346(2.965)	10.6(0.005)	
20	0.968(0.005)	0.984(0.121)	25.347(2.602)	10.7(0.003)	0.972(0.006)	1.942(0.282)	40.145(3.291)	10.8(0.005)	
QPADM-slack		$(n, p) = (200000, 500)$				QPADM-slack		$(n, p) = (500000, 1000)$	
K	CAR	CT	NI	NTSF	CAR	CT	NI	NTSF	
5	0.975(0.005)	2.300(0.300)	20.012(2.100)	10.4(0.004)	0.972(0.005)	4.750(0.650)	30.721(3.100)	10.7(0.005)	
10	0.973(0.006)	1.580(0.220)	23.113(2.400)	10.5(0.004)	0.969(0.006)	2.930(0.390)	35.946(3.250)	10.9(0.008)	
20	0.961(0.008)	1.050(0.150)	25.947(2.900)	11.0(0.006)	0.965(0.009)	2.010(0.340)	44.745(3.600)	11.1(0.008)	
QPADM-slack(GB)		$(n, p) = (200000, 500)$				QPADM-slack(GB)		$(n, p) = (500000, 1000)$	
K	CAR	CT	NI	NTSF	CAR	CT	NI	NTSF	
5	0.978(0.004)	2.270(0.285)	19.812(2.000)	10.3(0.003)	0.975(0.004)	4.720(0.620)	30.521(3.000)	10.6(0.004)	
10	0.976(0.005)	1.550(0.205)	22.913(2.300)	10.4(0.003)	0.971(0.005)	2.900(0.370)	35.746(3.150)	10.8(0.007)	
20	0.964(0.007)	1.020(0.140)	25.747(2.800)	10.9(0.005)	0.968(0.008)	1.980(0.320)	44.545(3.500)	11.0(0.007)	
M-QPADM-slack(GB)		$(n, p) = (200000, 500)$				M-QPADM-slack(GB)		$(n, p) = (500000, 1000)$	
K	Nonzero	AE	Ite	Time	Nonzero	AE	Ite	Time	
5	0.980(0.003)	2.250(0.270)	19.612(1.900)	10.2(0.002)	0.977(0.003)	4.700(0.600)	30.321(2.900)	10.5(0.003)	
10	0.978(0.004)	1.530(0.190)	22.713(2.200)	10.3(0.002)	0.973(0.004)	2.880(0.350)	35.546(3.050)	10.7(0.006)	
20	0.966(0.006)	1.000(0.130)	25.547(2.700)	10.8(0.004)	0.970(0.007)	1.960(0.300)	44.345(3.400)	10.9(0.006)	

4.1 Synthetic Data

We carried out a series of numerical experiments to showcase the robustness of the proposed algorithm. In this subsection, we solely concentrate on the experiments involving large-scale data. The large-scale

classification data are generated from the distributions $N(\boldsymbol{\mu}_+, \Sigma)$ and $N(\boldsymbol{\mu}_-, \Sigma)$, respectively, where $\boldsymbol{\mu}_+ = (1, \dots, 1, 0, \dots, 0)^\top$ with the first 10 elements being 1 and the rest being 0, $\boldsymbol{\mu}_- = (-1, \dots, -1, 0, \dots, 0)^\top$ with the first 10 elements being -1 and the rest being 0, and the covariance matrix is

$$\Sigma = \begin{bmatrix} \Sigma_{10}^* & \mathbf{0} \\ \mathbf{0} & \mathbf{I}_{(p-10)} \end{bmatrix}. \quad (4.3)$$

Here, Σ_{10}^* is a 10×10 matrix with all diagonal elements being 1 and the rest being $\rho < 1$. Note that the larger ρ implies the higher correlation between the first 10 features of the input data. This data has been used in Liang et al. (2024) for SVMs. Here, we implement our experiments on $\rho = 0.5$. Clearly, the first 10 features play a key role on the classification boundary. For this example, the Bayes classifier is $F = \sum_{j=1}^{10} x_j$. To further demonstrate the stability of the proposed algorithm, we added noise in a manner similar to that described in Wu et al. (2025d). The labels of the noise points are chosen from $\{+, -\}$ with equal probability. The positions of these noised points are generated from Gaussian distribution $N(\boldsymbol{\mu}_n, \Sigma_n)$ with $\boldsymbol{\mu}_n = (0, 0, \dots, 0)^\top$ and $\Sigma_n = \Sigma$. These noised points affect the labels around the boundary and the level of the noise is controlled by the ratio of the noise data in the training set, denoted by $\alpha(\%)$. Note that the noise does not change the Bayes classifier, but it can affect the result of estimated classifier. Here we fix α at 20%. We set the number of training samples to $n = 200000$ and $n = 500000$, the number of testing samples to $m = 1000000$, and the data dimensions (p) to 500 and 1000.

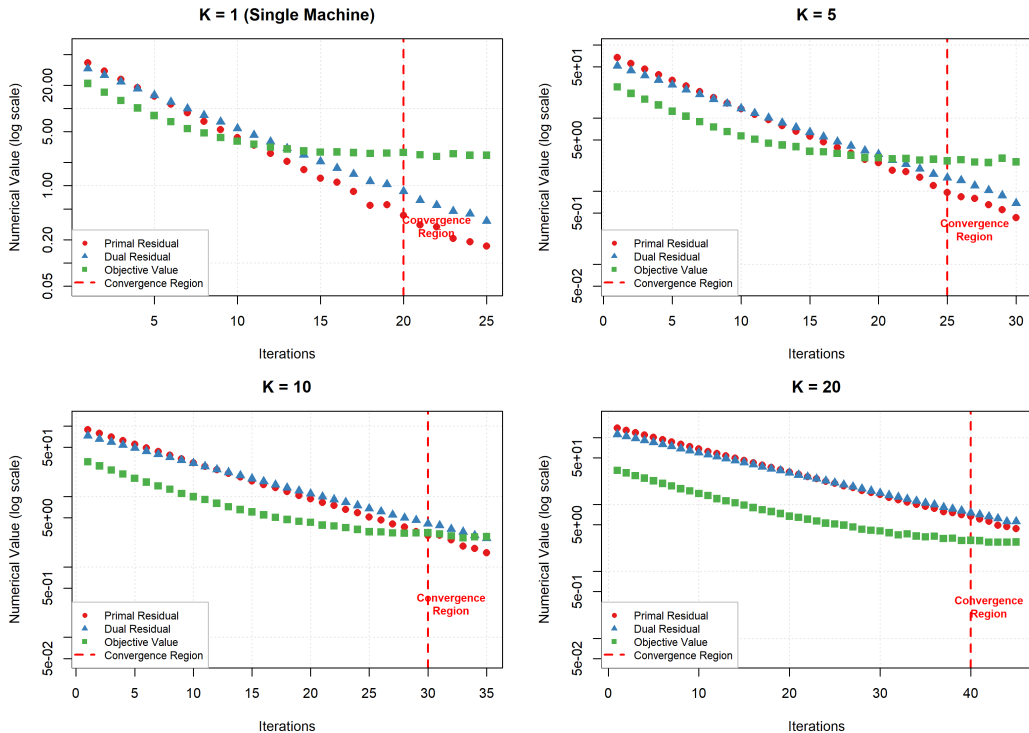


Figure 2: Parallel ADMM convergence performance with different numbers of sub-machines.

The true coefficients under consideration exhibit sparse blockiness. Here, we employ our parallel algorithm, named PADMM, to load SFL-SVM for data training. Other parallel algorithms for large-scale

SVM computation are presented in Guan et al. (2020) and Wu et al. (2025b). As described in Wu et al. (2025b), the parallel SVM algorithm in Guan et al. (2020) is referred to as QPADM-salck, while the two in Wu et al. (2025b) are named QPADM-slack(GB) and M-QPADM-slack(GB). Table 7 records the averaged results of 100 runs. Abbreviations in the table: CT for computation time, CAR for classification accuracy rate, NI for the number of iterations, and NTSF for the number of true selected features. A more detailed analysis follows.

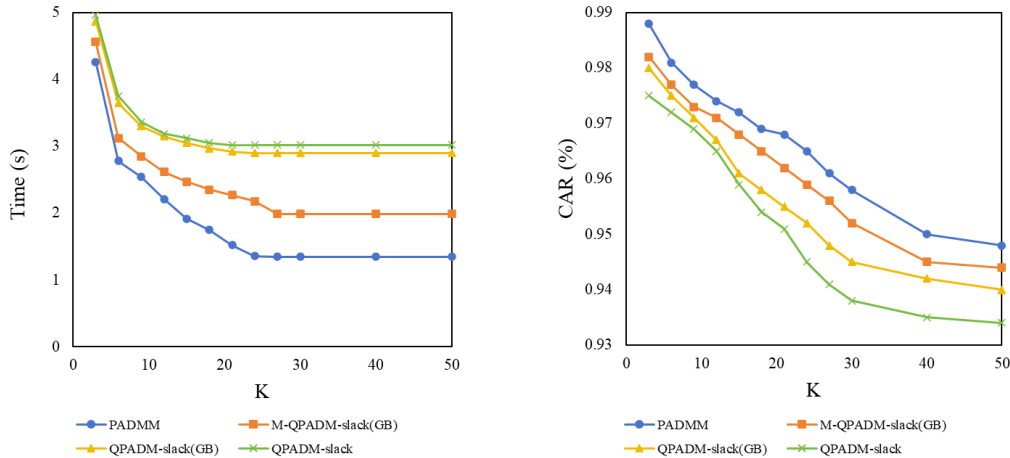


Figure 3: A schematic diagram depicting the variations of computation time and classification accuracy rate of four parallel algorithms with the number of sub-machines.

Analysis of the data in the table for different parallel algorithms (PADMM, QPADM-slack, QPADM-slack(GB), and M-QPADM-slack(GB)) under two data configurations ($(n, p) = (200000, 500)$ and $(n, p) = (500000, 1000)$) across various metrics reveals the following: PADMM exhibits the best overall performance, boasting the highest CAR, relatively low CT, fewer NI, and a stable NTSF close to 10. As the value of K increases, the CAR generally declines for all algorithms, while the CT mostly decreases and the NI increases. As Wu et al. (2025b) and Wu et al. (2025c) stated, this undesirable phenomenon does not result from the inherent defects of the algorithm itself. Instead, it stems from the consensus constraints in constructing the parallel computing results. This consensus structure leads to poorer algorithm performance as the number of sub-machines increases. When the data scale increases from $(n, p) = (200000, 500)$ to $(n, p) = (500000, 1000)$, the CAR of all algorithms slightly decreases, and both the CT and NI increase significantly, indicating that larger data volumes pose challenges to classification and computational performance. Although the PADMM algorithm proposed in this paper tends to deteriorate at large scales, it is more robust and scalable compared to other algorithms. In Figure 2, we present the convergence of the proposed PADMM under different numbers of sub-machines when the data size is $(n, p) = (500000, 1000)$. Apparently, the proposed algorithm converges rapidly with different numbers of sub-machines. However, as the number of sub-machines rises, the convergence speed tends to slow down, which aligns with the increase in IN as the number of machines increases in Table 7.

In Table 7, only the cases with 5, 10 and 20 sub-machines are presented. The results of parallel computing with more sub-machines are shown in Figure 3. Figure 3 reports the schematic diagrams of the changes in computation time and classification accuracy as K increases. Regarding the computation time in Figure 3, when K is greater than 20, the computation time tends to stabilize and no longer decreases. The reason for this is that the memory of the machine used in our experiment is limited, and it can only support the parallel operation of about 20 machines at a time. If there are more machines,

due to insufficient memory, the acceleration effect cannot be achieved. As for CAR, it keeps decreasing as the number of machines increases. This is still due to the drawbacks of the consensus structure. When the number of sub-machines increases, the accuracy of the iterative solution will decline.

4.2 Real Data

To empirically validate the generality and effectiveness of the distributed algorithm proposed in this study, we selected the publicly available benchmark dataset FMA (Free Music Archiv) in the field of music information retrieval as the verification platform. This selection was made after careful consideration for the following reasons: Firstly, the rich musical features provided by the FMA dataset inherently possess various structural information, which perfectly suits the application of the CR-SVMs model. Secondly, although the tracks in FMA may have multi-label attributes, through close collaboration with music domain experts, we determined an authoritative “primary genre” label for each piece of music, thus constructing a clear large-scale single-label music classification task. This task is not only large-scale enough to demonstrate the necessity of distributed computing, but its high-dimensional feature space and inherent structural characteristics also serve as an ideal testbed for examining whether the new algorithm can effectively perform sparse modeling and accurate classification in complex real-world scenarios.

The FMA dataset is a public music analysis dataset with various music features and metadata, which can be found in the GitHub repository (<https://github.com/mdeff/fma>) and comes in multiple versions. The small subset we commonly use, namely `fma.small`, consists of 8 categories, with 1000 audio samples in each category, totaling 8000 audio samples. It should be noted that in the “features.csv” of FMA, the feature names already include the feature types. We can group them by the prefixes of the feature names. We group the 1036 features according to their physical meanings. Specifically, we can divide the features into the following 7 groups: 16 time-domain features (including `zcr_mean`, `zcr_var`, `rms_mean`, `rms_var`, etc.), 32 spectral features (including the mean and variance of `spectral_centroid`, `spectral_bandwidth`, `spectral_rolloff`, `spectral_flatness`, etc.), 160 MFCC features (including statistics such as the mean and variance of 20 MFCC coefficients), 96 chroma features (including statistics such as the mean and variance of 12 chroma features), 48 tonnetz features (including statistics such as the mean and variance of 6 tonnetz features), 518 echonest features (including a comprehensive feature set from the echonest audio analysis engine), and 166 other features (including rhythm features (tempo), beat features (beat), and other audio features that are not classified into the above six main categories).

4.2.1 Classification accuracy

In each training session, we randomly select two out of eight categories, each with 1000 samples. We randomly select 800 samples from each category as the training set and the remaining 200 test samples. With these samples, we respectively employ the PADMM algorithm (loaded with SGL-SVM) presented in this paper, the QPADM-slack algorithm (loaded with SCAD-SVM) proposed by Guan et al. (2020), and the QPADM-slack(GB) algorithm (loaded with SCAD-SVM) proposed by Wu et al. (2025b) to train predictive SVMs and achieved predictive performance on the test set. To evaluate the algorithms, several performance metrics are defined. The metrics include: (1) “Sparsity”, defined as the proportion of zero coefficients (i.e., the number of zero coefficients divided by the total number of coefficients); (2) “Train”, which quantifies the classification accuracy on the training set; and (3) “Test”, which measures the classification accuracy on the testing set. In addition, we present the results of running algorithms in parallel on different numbers of sub-machines. Each experimental setting is independently simulated 100

times, and the average results are reported in Table 8.

Table 8: Comparative analysis of sparsity, training, and testing accuracies (%) among PADMM, QPADM-slack and QPADM-slack(GB) algorithms

K	PADMM			QPADM-slack(GB)			QPADM-slack		
	Sparsity	Train	Test	Sparsity	Train	Test	Sparsity	Train	Test
2	90.38	99.32	97.27	85.99	95.14	92.96	83.64	93.38	92.00
4	90.37	99.26	97.15	84.61	94.57	92.04	81.37	92.27	91.06
6	90.36	99.17	97.08	83.60	93.89	91.48	80.14	91.78	90.60
8	90.32	99.04	96.93	82.11	93.05	90.95	79.37	91.06	89.93
10	90.13	98.91	96.84	81.37	92.58	90.09	77.99	90.78	89.09
12	90.03	98.79	96.71	80.76	91.89	89.40	77.13	90.03	88.38
14	89.87	98.61	96.59	79.37	91.17	88.66	76.43	89.74	87.84
16	89.60	98.50	96.42	78.70	90.37	87.41	73.96	88.38	87.07
18	89.67	98.44	96.38	77.66	89.80	86.29	72.66	87.79	86.26
20	89.57	98.34	96.27	76.26	88.64	85.35	71.46	87.67	85.18

The table presents a comparative analysis of the sparsity, training accuracy, and testing accuracy of three algorithms, namely PADMM, QPADM-slack, and QPADM-slack(GB), under different numbers of machines K . Regarding sparsity, all three algorithms show a decreasing trend as the value of K increases. Among them, the PADMM algorithm consistently exhibits the highest sparsity with a relatively smaller decline, while the QPADM-slack algorithm experiences the most significant decrease. This indicates that the PADMM algorithm has a distinct advantage in generating sparse models. In terms of training accuracy and testing accuracy, both also gradually decline as the value of K increases. At the same K value, the PADMM algorithm outperforms the other two algorithms in both aspects, suggesting that it has better classification performance on the training set and stronger generalization ability on the testing set. Overall, the PADMM algorithm demonstrates superior comprehensive performance. Additionally, an increase in the value of K may lead to an increase in model complexity and negatively impact the algorithm’s performance. Therefore, in practical applications, an appropriate value of K needs to be selected to balance the model’s sparsity and classification performance.

Next, we report the influence of the previous seven pre-grouped sets on the accuracy of audio data classification. Regarding the coefficient estimation of SGL-SVM, the MFCC feature group has the largest number of non-zero estimated coefficients, followed by the spectral feature group, and then the chroma feature group. We have presented the sum of the absolute values of the estimated coefficients for each feature group and the schematic diagrams of the estimated coefficient distributions in Figures 4 and 5. In coefficient estimation, the number of non-zero coefficients also represents the importance of feature values. Based on music background knowledge, the MFCC feature group is the most important as it mimics human auditory perception and can effectively capture timbre and sound quality features. The spectral feature group comes next because it describes the spectral shape and energy distribution. The chroma feature group captures harmony and tonality information and also plays a relatively important role in music classification. Compared with these three groups, when the regularization penalty is relatively large, the other four feature groups have very few non-zero estimated coefficients, which can even be

ignored. Therefore, when storage resources are limited, only these three feature groups can be collected to train a machine learning model for audio classification.

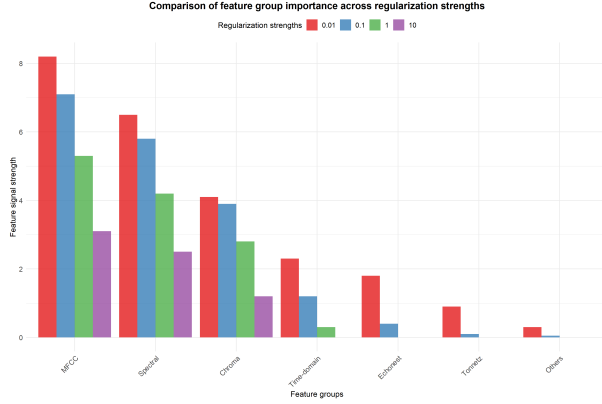


Figure 4: Group weight norms under different penalty parameters.

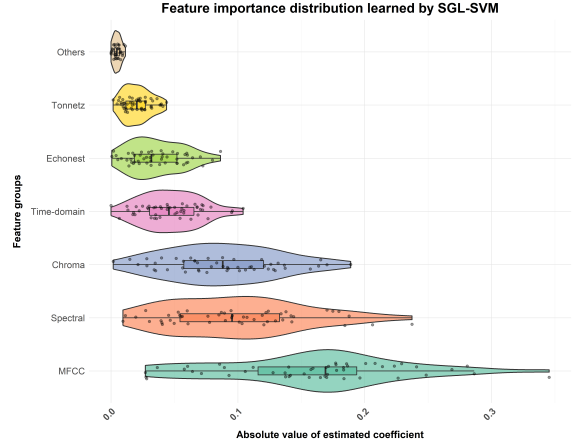


Figure 5: Feature group weight distribution.

5 Conclusion

This paper addresses the issue of insufficient research on distributed parallel algorithms for CR-SVMs. Based on convex and non-convex SVM problems, the paper proposes a unified optimization framework, derives the corresponding parallel ADMM algorithm, and proves its global convergence with an improved sublinear rate. Meanwhile, to ensure the completeness of the work, we also propose a SGL-SVM model, which applies the sparse group lasso to SVM classification and can effectively handle data with group structures. Regardless of the regularization terms and SVM loss functions used, the computational complexity of our proposed algorithm remains consistent, which fully demonstrates its universality. Experiments on simulated data and the FMA dataset verify the reliability, stability, and scalability of the algorithm. Moreover, numerical experiments indicate that when training a machine learning model for music data classification, the MFCC feature group is the most crucial, followed by the spectral feature group and then the chroma feature group.

Note that the algorithm proposed in this paper mainly focuses on convex loss functions. As for non-convex loss functions (refer to Wang and Li (2025) and its references), we plan to solve them in future work. There are many other directions for further research in the future. At the theoretical level, future research will focus on enhancing the algorithm’s efficiency and improving its theoretical foundation. Specifically, it includes investigating the algorithm’s convergence properties under more challenging conditions such as, noisy or incomplete data and deriving more precise convergence rate estimates. Moreover, the algorithm’s structure can be optimized and combined with other techniques, such as stochastic gradient descent or advanced acceleration methods (Guo et al. (2020)) to improve its convergence speed and overall performance. In terms of applications, we can extend the framework to multi-label tasks (Zhang et al. (2021)), such as music auto-tagging, to further test its broad effectiveness.

CRediT authorship contribution statement

Rongmei Liang: Writing–original draft, Software, Methodology, Data curation. Zizheng Liu: Writing–review and editing, Data curation, Funding acquisition. Xiaofei Wu: Validation, Supervision, Project administration. Jingwen Tu: Funding acquisition, Visualization, Investigation.

Acknowledgements

We are very grateful to Professor Bingsheng He for his valuable discussions with us, which greatly helps us use the parallel ADMM algorithms to solve regression problems. The research of Liang and Wu was supported by the Scientific and Technological Research Program of Chongqing Municipal Education Commission [Grant Numbers KJQN202302003]. The research of Tu was supported by the General Program of Chongqing Natural Science Foundation [Grant Numbers CSTB2024NSCQ-MSX0077], the Doctoral Project of Chongqing Social Science Planning [Grant Numbers 2022BS064] and the Scientific and Technological Research Program of Chongqing Municipal Education Commission [Grant Numbers KJQN202301541].

References

- N. Becker, G. Toedt, P. Lichter, and A. Benner. Elastic scad as a novel penalization method for svm classification tasks in high-dimensional data. *BMC Bioinf.*, 12:138 – 138, 2011.
- S. Boyd, N. Parikh, E. Chu, B. Peleato, and J. Eckstein. Distributed Optimization and Statistical Learning Via the Alternating Direction Method of Multipliers. *Found. Trends Mach. Learn.*, 3(1): 1–122, 2010.
- C. Chen, B. He, Y. Ye, and X. Yuan. The direct extension of ADMM for multi-block convex minimization problems is not necessarily convergent. *Math. Program.*, 155(1-2):57–79, 2016.
- W. Deng, M.-J. Lai, Z. Peng, and W. Yin. Parallel multi-block admm with $o(1/k)$ convergence. *J. Sci. Comput.*, 71:712 – 736, 2013.
- C. Du, C. Du, S. Zhe, A. Luo, Q. He, and G. Long. Bayesian Group Feature Selection for Support Vector Learning Machines. In *Adv. Knowl. Discovery Data Min.*, pages 239–252. Springer International Publishing, 2016a.
- G. Du, S. Tian, Y. Qiu, and C. Xu. Effective and efficient grassfinch kernel for svm classification and its application to recognition based on image set. *Chaos, Solitons & Fractals*, 89:295–303, 2016b.
- J. Fan and R. Li. Variable Selection via Nonconcave Penalized Likelihood and its Oracle Properties. *J. Am. Stat. Assoc.*, 96(456):1348–1360, 2001.
- J. H. Friedman, T. J. Hastie, and R. Tibshirani. A note on the group lasso and a sparse group lasso. *arXiv: Statistics Theory*, 2010.
- Y. Gu, J. Fan, L. Kong, S. Ma, and H. Zou. ADMM for High-Dimensional Sparse Penalized Quantile Regression. *Technom.*, 60(3):319–331, 2018.
- L. Guan, T. Sun, L. Qiao, Z. Yang, D. Li, K. Ge, and X. Lu. An efficient parallel and distributed solution to nonconvex penalized linear SVMs. *Front. Inf. Technol. Electron. Eng.*, 21:587–603, 2020.

- H. Guo, A. Zhang, and W. Wang. An accelerator for online svm based on the fixed-size kkt window. *Eng. Appl. Artif. Intell.*, 92:103637, 2020.
- B. He, M. Tao, and X. Yuan. Alternating direction method with gaussian back substitution for separable convex programming. *SIAM J. Optim.*, 22(2):313–340, 2012.
- Y. Huo, L. Xin, C. Kang, M. Wang, Q. Ma, and B. Yu. Sgl-svm: A novel method for tumor classification via support vector machine with sparse group lasso. *J. Theor. Biol.*, 486:110098, 2020.
- R. Langone, C. Alzate, B. De Ketelaere, J. Vlasselaer, W. Meert, and J. A. Suykens. Ls-svm based spectral clustering and regression for predicting maintenance of industrial machines. *Eng. Appl. Artif. Intell.*, 37:268–278, 2015.
- W. Li, W. Shan, and M. Liu. A distributed algorithm for fuzzy support vector machine on multi-source data-driven credit scoring. *Eng. Appl. Artif. Intell.*, 143:110009, 2025.
- R. Liang, X. Wu, and Z. Zhang. Linearized Alternating Direction Method of Multipliers for Elastic-net Support Vector Machines. *Pattern Recognit.*, 148:110134, 2024.
- Y. Saad. *Iterative Methods for Sparse Linear Systems*. Society for Industrial and Applied Mathematics, second edition, 2003.
- F. Tang, L. Adam, and B. Si. Group feature selection with multiclass support vector machine. *Neurocomput.*, 317:42–49, 2018.
- R. Tibshirani, M. Saunders, S. Rosset, J. Zhu, and K. Knight. Sparsity and Smoothness Via the Fused Lasso. *J. Roy. Stat. Soc. Ser. B. (Stat. Method.)*, 67(1):91–108, 2005.
- V. N. Vapnik. *The Nature of Statistical Learning Theory*. Springer, 1995.
- H. Wang and W. Li. Sparse and robust elastic net support vector machine with bounded concave loss for large-scale problems. *Eng. Appl. Artif. Intell.*, 162:112352, 2025.
- H. Wang and Y. Xu. Sparse elastic net multi-label rank support vector machine with pinball loss and its applications. *Appl. Soft Comput.*, 104:107232, 2021. ISSN 1568-4946.
- L. Wang, J. Zhu, and H. Zou. The doubly regularized support vector machine. *Stat. Sin.*, 16:589–615, 2006.
- L. Wang, J. Zhu, and H. Zou. Hybrid Huberized Support Vector Machines for Microarray Classification and Gene Selection. *Bioinf.*, 24(3):412–419, 2008.
- X. Wu, H. Ming, Z. Zhang, and Z. Cui. Multi-block Alternating Direction Method of Multipliers for Ultrahigh Dimensional Quantile Fused Regression. *Comput. Stat. Data Anal.*, 192:107901, 2024.
- X. Wu, Y. Chao, R. Liang, s. Tang, and Z. Zhang. Feature splitting parallel algorithm for Dantzig selectors. *Stat. Comput.*, 35(116), 2025a.
- X. Wu, D. Guo, R. Liang, and Z. Zhang. Parallel ADMM Algorithm with Gaussian Back Substitution for High-Dimensional Quantile Regression and Classification. *Stat. Comput.*, 35(139), 2025b.
- X. Wu, R. Liang, Z. Zhang, and Z. Cui. A unified consensus-based parallel ADMM algorithm for high-dimensional regression with combined regularizations. *Comput. Stat. Data Anal.*, 203:108081, 2025c.

- X. Wu, R. Liang, Z. Zhang, and Z. Cui. Multi-block linearized alternating direction method for sparse fused Lasso modeling problems. *Appl. Math. Modell.*, 137:115694, 2025d. ISSN 0307-904X.
- B. Xing, K. Zhang, S. Sun, L. Zhang, Z. Gao, J. Wang, and S. Chen. Emotion-driven chinese folk music-image retrieval based on de-svm. *Neurocomput.*, 148:619–627, 2015.
- Y. Xu, I. G. Akrotirianakis, and A. Chakraborty. Proximal gradient method for huberized support vector machine. *Pattern Anal. Appl.*, 19:989–1005, 2015.
- Y. Yang and H. Zou. An Efficient Algorithm for Computing the HHSVM and Its Generalizations. *J. Comput. Graphical Stat.*, 22(2):396–415, 2013.
- G.-B. Ye and X. Xie. Split Bregman method for large scale fused Lasso. *Comput. Stat. Data Anal.*, 55(4):1552–1569, 2011. ISSN 0167-9473.
- M. Yuan and Y. Lin. Model selection and estimation in regression with grouped variables. *J. Roy. Stat. Soc. Ser. B. (Stat. Method.)*, 68(1), 2006.
- C. Zhang. Nearly Unbiased Variable Selection Under Minimax Concave Penalty. *Ann. Stat.*, 38(2): 894–942, 2010.
- X. Zhang, Y. Wu, L. Wang, and R. Li. Variable selection for support vector machines in moderately high dimensions. *J. Roy. Stat. Soc. Ser. B. (Stat. Method.)*, 78(1):53–76, 2016.
- Y. Zhang, J. Yu, X. Dong, and P. Zhong. Multi-task support vector machine with pinball loss. *Eng. Appl. Artif. Intell.*, 106:104458, 2021. ISSN 0952-1976.
- J. Zhu, S. Rosset, R. Tibshirani, and T. Hastie. 1-norm support vector machines. In S. Thrun, L. Saul, and B. Schölkopf, editors, *Adv. Neural Inf. Process. Syst.*, volume 16, Vancouver, British Columbia, Canada, 2003. MIT Press.
- W. Zhu, Y. Song, and Y. Xiao. Support vector machine classifier with huberized pinball loss. *Eng. Appl. Artif. Intell.*, 91:103635, 2020. ISSN 0952-1976.
- H. Zou. The Adaptive Lasso and Its Oracle Properties. *J. Am. Stat. Assoc.*, 101:1418–1429, 2006.
- H. Zou and T. Hastie. Regularization and Variable Selection Via the Elastic Net. *J. Roy. Stat. Soc. Ser. B. (Stat. Method.)*, 67(2):301–320, 2005.
- H. Zou and R. Li. One-step Sparse Estimates in Nonconcave Penalized Likelihood Models. *Ann. Stat.*, 36(4):1509–1533, 2008.